



Cloud condensation nuclei activity, closure, and droplet growth kinetics of Houston aerosol during the Gulf of Mexico Atmospheric Composition and Climate Study (GoMACCS)

Sara Lance,^{1,2} Athanasios Nenes,¹ Claudio Mazzoleni,³ Manvendra K. Dubey,⁴ Harmony Gates,⁵ Varuntida Varutbangkul,⁵ Tracey A. Rissman,⁵ Shane M. Murphy,⁵ Armin Sorooshian,⁵ Richard C. Flagan,⁵ John H. Seinfeld,⁵ Graham Feingold,² and Hafliði H. Jonsson⁶

Received 31 December 2008; revised 9 April 2009; accepted 13 May 2009; published 30 July 2009.

[1] In situ cloud condensation nuclei (CCN) measurements were obtained in the boundary layer over Houston, Texas, during the 2006 Gulf of Mexico Atmospheric Composition and Climate Study (GoMACCS) campaign onboard the CIRPAS Twin Otter. Polluted air masses in and out of cloudy regions were sampled for a total of 22 flights, with CCN measurements obtained for 17 of these flights. In this paper, we focus on CCN closure during two flights, within and downwind of the Houston regional plume and over the Houston Ship Channel. During both flights, air was sampled with particle concentrations exceeding $25,000\text{ cm}^{-3}$ and CCN concentrations exceeding $10,000\text{ cm}^{-3}$. CCN closure is evaluated by comparing measured concentrations with those predicted on the basis of measured aerosol size distributions and aerosol mass spectrometer particle composition. Different assumptions concerning the internally mixed chemical composition result in average CCN overprediction ranging from 3% to 36% (based on a linear fit). It is hypothesized that the externally mixed fraction of the aerosol contributes much of the CCN closure scatter, while the internally mixed fraction largely controls the overprediction bias. On the basis of the droplet sizes of activated CCN, organics do not seem to impact, on average, the CCN activation kinetics.

Citation: Lance, S., et al. (2009), Cloud condensation nuclei activity, closure, and droplet growth kinetics of Houston aerosol during the Gulf of Mexico Atmospheric Composition and Climate Study (GoMACCS), *J. Geophys. Res.*, *114*, D00F15, doi:10.1029/2008JD011699.

1. Introduction

[2] In addition to human health and direct climate radiative forcing implications, aerosols play an important role in the formation of clouds, as they provide the sites upon which cloud droplets form. Higher aerosol concentrations generally lead to a greater number of cloud droplets, but not all particles are equally efficient cloud condensation nuclei (CCN). Each particle requires exposure to a threshold water

vapor concentration, termed “critical supersaturation,” before acting as a cloud condensation nucleus (CCN) and spontaneously activating into a cloud droplet. The complexity of aerosol-cloud interactions, and the strong impact of clouds on the planetary radiative budget leads to an “aerosol indirect climate effect” that constitutes the largest source of uncertainty in assessments of anthropogenic climate change [Forster *et al.*, 2007].

[3] The conditions under which a particle can act as a CCN depend strongly on particle size [e.g., Seinfeld and Pandis, 2006] although particle composition also plays an important role. The latter effects are a challenge for predictive models, as they require simulating the evolution of the aerosol population as it ages and interacts with fresh emissions. Dusek *et al.* [2006] suggest that the aerosol composition has only a minor effect on CCN concentrations, with variability in the size distribution alone accounting for 84–96% of the variability in CCN concentrations. Wang [2007] showed that cloud albedo is insensitive to particle composition. Others however have found that the mass fraction of one type of chemical compounds, known as hydrocarbon-like organic aerosol (HOA), can explain up to 40% of the CCN concentration variability [Quinn *et al.*,

¹School of Earth and Atmospheric Sciences and School of Chemical and Biomolecular Engineering, Georgia Institute of Technology, Atlanta, Georgia, USA.

²Chemical Sciences Division, National Oceanic and Atmospheric Administration, Boulder, Colorado, USA.

³Department of Physics, Michigan Technological University, Houghton, Michigan, USA.

⁴Climate Observations, Los Alamos National Laboratory, Los Alamos, New Mexico, USA.

⁵Department of Chemical Engineering, California Institute of Technology, Pasadena, California, USA.

⁶Center for Inter-Disciplinary Remotely Piloted Aircraft Studies, Naval Postgraduate School, Marina, California, USA.

2008]. *Furutani et al.* [2008] also found that changes in aerosol composition from aging processes can have an important effect on CCN activity.

[4] To predict CCN concentrations for a given particle size distribution, simplifying assumptions are typically made for the chemical composition of the aerosol population; this is the case even when composition measurements are available, since no measurement technique is capable of quantifying the full array of compounds present in ambient aerosol [*Saxena and Hildemann*, 1996]. Solubility, density, molecular weight, and surfactant properties all affect CCN activity [*Saxena and Hildemann*, 1996], as do interactions between the organic and inorganic aerosol constituents [*Shulman et al.*, 1996; *Dinar et al.*, 2008]. Most often, Aerodyne Aerosol Mass Spectrometer (AMS) measurements are used to constrain the chemical properties of the soluble inorganic fraction of ambient aerosol (nitrate, sulfate and ammonium ions) for CCN studies [e.g., *Cubison et al.*, 2008; *Ervens et al.*, 2007; *Medina et al.*, 2007]. However, AMS measurements are unable to provide the refractory composition (e.g., soot) or complete speciation of the organic fraction. Numerous simple approaches have been proposed, on the basis of activation spectra or hygroscopic uptake properties of carbonaceous aerosol, to characterize the impact of organics on water activity and CCN activity [e.g., *Petters and Kreidenweis*, 2007; *Vestin et al.*, 2007; *Padró et al.*, 2007]. Although very useful for parameterizing ambient data measurements, these methods are often applied with the assumption that the organic fraction is water-soluble and does not affect surface tension behavior, both of which result in inferred hygroscopicity that may not reflect the properties of the water-soluble carbonaceous fraction of the aerosol [e.g., *Engelhart et al.*, 2008; *Asa-Awuku et al.*, 2009].

[5] Apart from the diversity of organic compounds present in ambient aerosol, another important source of uncertainty in predicting CCN concentrations is the mixing state of the aerosol population, especially close to emission sources. Modeling studies often assume that particles are internally mixed (i.e., all particles of a given size have the same composition); in reality, close to sources, the aerosol is often an external mixture, and chemical composition varies among particles of the same size. Since the soluble (typically inorganic) components dominate the water-uptake properties of the aerosol, the existence of externally mixed hydrophobic particles can have an important impact on CCN number.

[6] CCN closure studies have been performed over the last decade to evaluate the predictive understanding of the aerosol-CCN link [e.g., *VanReken et al.*, 2003; *Chang et al.*, 2007; *Cantrell et al.*, 2001; *Medina et al.*, 2007; *Broekhuizen et al.*, 2006; *Ervens et al.*, 2007, and references therein]. These studies use measurements of the aerosol size distribution and chemical composition to predict the number of CCN for a given supersaturation; direct in situ observations of CCN (obtained by exposing the ambient particles to a controlled water vapor supersaturation) are then compared against these predictions. Most often, CCN concentration is overpredicted on average by less than $\sim 30\%$; the variability however is often much larger and difficult to account for.

[7] The current work focuses on CCN measurements taken onboard the Center for Interdisciplinary Remotely Piloted Aircraft Studies (CIRPAS, <http://www.cirpas.org>)

Twin Otter during the Gulf of Mexico Atmospheric Composition and Climate Study (GoMACCS) field campaign in Houston, Texas, from 25 August to 15 September 2006 (<http://esrl.noaa.gov/csd/2006/>). Owing to a combination of motor vehicle traffic, close proximity to large petrochemical refineries, chemical plants, waste treatment, coal-fired power plants, and heavy industrial shipping via the Houston Ship Channel, measured aerosol concentrations often exceeded $10,000 \text{ cm}^{-3}$. Houston, with its diverse mixture of local industrial sources in combination with the local marine and biogenic emissions, is an especially challenging area in which to predict the effect of aerosols on clouds. We study the ability to predict CCN concentrations in a heavily polluted environment, in which organic concentrations are often high, and explore the role of the particle chemical composition in the variability and biases of our CCN predictions. This study is complementary to the study of *Quinn et al.* [2008], which took place over the same time period onboard the NOAA ship *Ronald H. Brown*, and, the study of *A. Asa-Awuku et al.* (Airborne cloud condensation nuclei measurements during the 2006 Texas Air Quality Study, submitted to *Journal of Geophysical Research*, 2009), which took place onboard the NOAA WP-3D airborne platform.

2. Data Set Description

2.1. Overview of Flights

[8] Figure 1a shows the flight tracks for the Twin Otter research flights (RF) analyzed, each of which occurred during daylight hours. A total of 22 flights were carried out, during which air masses were sampled in the vicinity of powerplants (RF9, 13, 14, 17, 19), the Houston Ship Channel (RF4, 11), downtown Houston (RF11, 13, 21, 22) and its surrounding areas. Supersaturation in the measurements varied from 0.3 to 1.0%, and CCN concentrations, from 200 to $15,000 \text{ cm}^{-3}$. Table 1 shows a summary of the flights, the major sources of pollution, and the dominant wind direction. *Lu et al.* [2008] describe the complete instrument payload on the Twin Otter during GoMACCS.

2.2. CCN Counter Measurements

[9] CCN concentrations were measured using a Droplet Measurement Technologies continuous flow streamwise thermal gradient CCN counter (CCNc) [*Roberts and Nenes*, 2005; *Lance et al.*, 2006] at 1-Hz time resolution. CCN were sampled through a manifold from which all other in situ aerosol observations were taken (except for the particle size distribution measurements, which will be discussed later). The common sampling manifold was located downstream of a ball valve set to sample either from the main inlet (Figure 1b) or downstream of a counterflow virtual impactor [*Noone et al.*, 1988; *Ogren et al.*, 1992], which selectively sampled droplets and large particles with diameters exceeding $\sim 5 \mu\text{m}$, and was switched on during constant altitude legs in-cloud. CCN measurements were obtained for the aerosol outside of cloud, and, for the cloud droplet residuals.

[10] The supersaturation within the CCNc is controlled by the sample and sheath flow rates, column pressure, inlet temperature, and the temperature difference between the bottom and top of the column. The uncertainty for each of

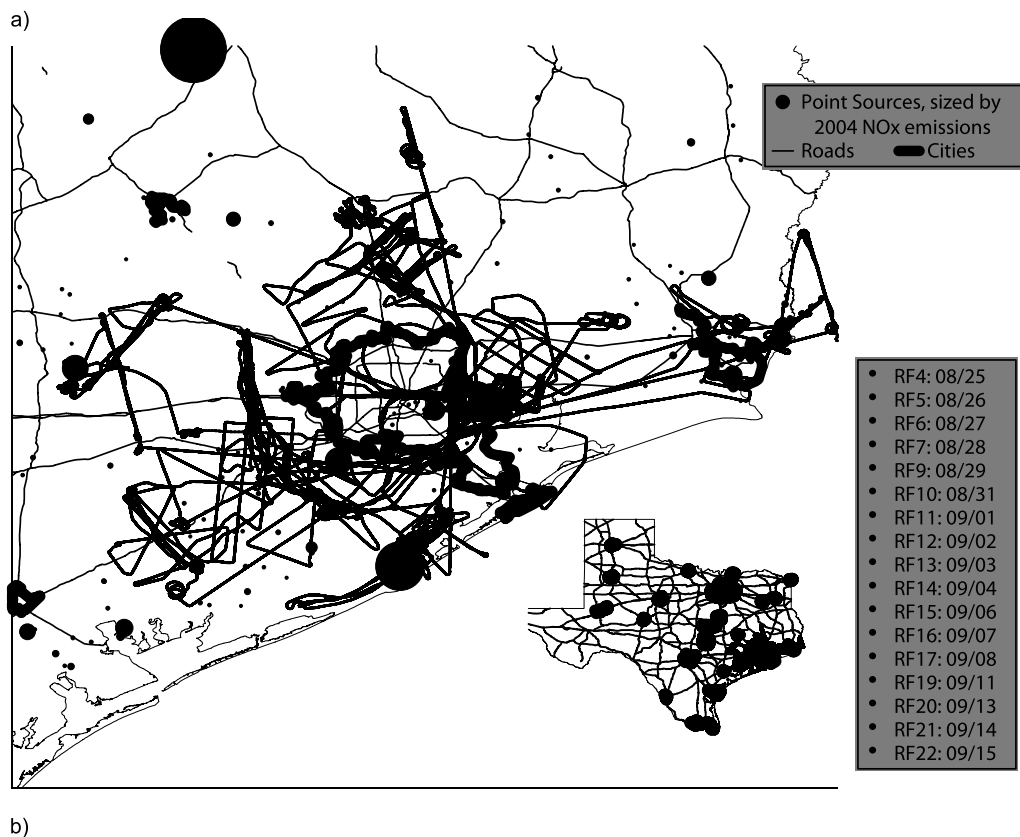


Figure 1. (a) Flight tracks for the Twin Otter research flights (RF) during which CCN measurements were available. Range shown is 27.9°N–31.4°N latitude, 93.5°W–97.0°W longitude. (b) Photograph of the Twin Otter (with the main inlet and CVI inlet indicated) (photo credit: Daniel Welsh-Bon) over a photograph of the industries along the Houston Ship Channel (photo credit: Armin Sorooshian).

these operating parameters is summarized in Table 2. The CCNc was operated throughout the campaign with a set flow rate of $\sim 1 \text{ L min}^{-1}$, consisting of sample and sheath flows with average rates of 0.092 and 0.909 L min^{-1} ,

respectively. The careful design of the Twin Otter main inlet (which decelerates the airflow by a factor of ten before it enters the sampling manifold) dampens most pressure oscillations; changes in attack angle of the aircraft still

Table 1. Twin Otter Science Flights During GoMACCS^a

Flight	Date	Mission Description	Wind Direction (From)	AMS Data Used	Supersaturation Range (%)	CCN Concentration Range (cm ⁻³)
RF1	21 Aug	Parish coal PP	E-SE	No		
RF2	22 Aug	Parish coal PP	E	No		
RF3	23 Aug	Parish coal PP	E	No		
RF4	25 Aug	Ship Channel	S-SE, NE	No	0.35–0.7	250–5000
RF5	26 Aug	Conroe	S, N-NE	No	0.4–0.7	200–800
RF6	27 Aug	Beaumont	S-SE	Yes	0.3–0.5	200–1000
RF7	28 Aug	Baytown	SW	Yes	0.5–1.0	500–5000
RF8	28 Aug		S	No		
RF9	29 Aug	Parish coal PP	W-NW	No	0.55–1.0	200–3000
RF10	31 Aug		N-NW	No	0.5–0.55	600–6000
RF11	1 Sep	Houston Ship Channel	N	No	0.35–0.85	250–10,000
RF12	2 Sep	Local BB	N-NE	Yes	0.5–0.55	600–9000
RF13	3 Sep	Houston, Parish coal PP	NE	No	0.45–0.5	1500–15,000
RF14	4 Sep	Parish coal PP	NE, NW	Yes	0.5–0.55	400–3000
RF15	6 Sep	Waste Treatment	N-NE	Yes	0.5–0.6	200–5000
RF16	7 Sep	Galveston	NE	Yes	0.35–0.9	200–6000
RF17	8 Sep	Parish coal PP	E-NE, W	No	0.4–0.9	250–9000
RF18	10 Sep		S	No		
RF19	11 Sep	Fayette coal PP	S, NW	No	0.45–0.55	150–1000
RF20	13 Sep	Conroe	N	No		350–7000
RF21	14 Sep	Houston, Parish	E-NE	Yes	0.45–0.55	200–15,000
RF22	15 Sep	Houston	S-SE	Yes	0.45–0.55	300–8000

^aNote that CCN data in first three flights are not available. PP, power plant; BB, biomass burning.

generate high-frequency (small amplitude) pressure fluctuations which are magnified by the active flow control in the CCNc and create flow oscillations in the growth chamber. To address this, a flow restriction upstream of the CCNc was used in most flights to dampen residual pressure fluctuations in the main sampling inlet. Without a flow restrictor (RF4), the sheath flow rate standard deviation increased by a factor of 4 (see Table 2). For RF7, the flow restrictor was replaced with a 0.33-m-long, 1.9-cm-diameter dead volume (with an added delay time of 4.4 s), which resulted in flow rate fluctuations comparable to leaving the flow restrictor off.

[11] Hegg *et al.* [2005] report that the transmission efficiency of the Twin Otter main inlet is close to 100% for particle diameters less than 3.5 μm . Similarly, particle losses through the flow restrictor have been found to be

negligible for submicron particles in the range of pressures and flow rates experienced during flight. Since nearly all CCN are below 300 nm, number losses for CCN in both the main inlet and in the flow restrictor upstream of the CCNc are negligible.

[12] In addition to pressure fluctuations, the CCNc is sensitive to low-frequency pressure changes during ascents and descents owing to the finite time required for the development of the temperature and supersaturation profiles within the instrument; this issue was addressed by maintaining the pressure at the inlet of the CCNc at ~ 700 mbar using a DMT Inlet Pressure Controller (<http://www.dropletmeasurement.com>). It consists of a vacuum pump with active flow control pulling downstream of the flow restrictor and in parallel to the CCNc. The pressure controller flow was set to maintain the pressure at the inlet

Table 2. Summary of CCNc Operation Characteristics

Flight	IPC On	Flow-Restrictor Present	Flight Category ^a	ΔT Variance (°C)	Q_{sh} Variance (cc min ⁻¹)	P Variance (mbar)	SS Variance (%)
RF4	No	No	2	0.50	19.4128	1.226	0.064
RF5	No	Yes	2	0.34	5.90161	1.657	0.052
RF6	No	Yes	2	0.06	4.71778	1.735	0.008
RF7	No	No	1	0.73	19.6443	1.068	0.095
RF9	No	Yes	2	0.76	3.51723	1.003	0.087
RF10	Yes	Yes	4	0.01	5.46324	1.906	0.003
RF11	Yes	Yes	3	0.01	5.44902	0.201	0.002
RF12	Yes	Yes	4	0.01	5.06662	1.669	0.002
RF13	Yes	Yes	4	0.01	5.61638	0.263	0.003
RF14	Yes	Yes	4	0.01	5.15539	1.639	0.003
RF15	Yes	Yes	4	0.01	4.43912	1.800	0.003
RF16	Yes	Yes	3	0.01	5.55128	0.909	0.003
RF17	Yes	Yes	3	0.01	4.88951	1.040	0.004
RF19	Yes	Yes	4	0.01	4.84348	1.514	0.003
RF20	Yes	Yes	4	0.01	4.94734	2.042	0.003
RF21	Yes	Yes	4	0.01	4.07664	1.886	0.003
RF22	Yes	Yes	4	0.01	4.31556	1.600	0.003

^aRefer to explanation of “flight category” in section 2.2.

of the CCNc to a constant value. The pressure controller was operated upstream of the CCNc for all but RF4, RF5, RF6, RF7 and RF9.

[13] The reduced pressure in the CCNc expands the sample volume and decreases the CCN concentration, requiring correction of the measured concentrations back to ambient concentrations, according to the ideal gas law

$$[CCN]_{amb} = [CCN]_{meas} \left(\frac{P_{amb}}{P_{CCN}} \right), \quad (1)$$

where $[CCN]_{amb}$ and $[CCN]_{meas}$ are the ambient and measured CCN concentrations, and P_{amb} and P_{CCN} are the ambient and CCNc pressures, respectively. As the inlet pressure controller was not installed until midway through the mission, supersaturation in the CCNc during RF4, RF5, RF6, RF7 and RF9 drifted with the ambient pressure. For these flights, data collected during altitude changes are not considered.

[14] In addition to pressure changes, the drifting temperature of the CCNc inside the fuselage of the Twin Otter can cause changes in the CCNc supersaturation. The CCNc control software sets the column temperature at the top (T1) to a constant offset above ambient temperature for the thermal electric coolers to operate efficiently. The temperature setpoints at the middle and bottom of the column (T2 and T3, respectively) are adjusted accordingly, to maintain a constant setpoint temperature difference (T3 – T1). For this study, the ambient temperature is the uncontrolled temperature within the unpressurized cabin of the aircraft, which heats up from the nearby pumps in an enclosed space and cools off as the aircraft ascends to higher altitudes. The T1 setpoint does not continuously follow ambient temperature, rather only when the ambient temperature exceeds 1°C difference from T1. Thus, the temperature setpoint increments in step changes as the ambient temperature drifts, which occasionally causes slight but abrupt changes in supersaturation.

[15] Uncertainty in the temperature difference between the bottom and top of the CCNc column translates directly to uncertainty in the CCNc supersaturation. The temperature uncertainty was significantly higher in the early flights compared to later flights, as shown in Table 2. Starting with the flight on 1 September 2006 (RF11), a new AC/DC power supply was installed, which significantly reduced the temperature fluctuations recorded by the thermistors in the CCNc, bringing the temperature variability down to levels observed in laboratory experiments and ground-based studies. The high-frequency variability in recorded temperatures in the earlier flights cannot be real (as the thermal resistance in the flow column does not permit such high-frequency fluctuations) and is likely a result of electronic noise; nevertheless, we treat the measured temperature uncertainty as true, leading to significantly higher supersaturation uncertainty (Table 2).

[16] For several of the research flights (RF7, RF11, RF16 and RF17) the CCNc was operated at multiple supersaturations by periodically making step changes in the vertical (streamwise) temperature gradient. The temperature gradient cycling was automated and was not, therefore, purposely aligned with the sampling of plumes. For flights after 31

August, the supersaturation was maintained at $0.5 \pm 0.03\%$ (one standard deviation).

[17] The CCNc supersaturation was calibrated throughout the mission at various pressures, flow rates, and temperature gradients using laboratory-generated ammonium sulfate particles (following the SMCA procedure of A. Nenes and J. Medina (Scanning mobility CCN analysis: A method for fast measurements of size-resolved CCN activity and growth kinetics, submitted to *Aerosol Science and Technology*, 2009) and *Asa-Awuku et al.* [2009]). These calibrations were then used to determine the supersaturation at different operating conditions during flight, interpolating between the calibrated supersaturations when required using the thermal efficiency and supersaturation parameterizations from *Lance et al.* [2006]. The slope and intercept of the supersaturation versus ΔT curve were accounted for in the calculations of thermal resistance, assuming a van't Hoff factor of 2.5 and spherical shape for the dry ammonium sulfate calibration aerosol [*Rose et al.*, 2008; *Zelenyuk et al.*, 2006].

[18] Figure 2 shows a summary of the operating conditions and the variability therein for four representative flights (RF7, RF9, RF11, RF19). The uncertainty in their operating conditions can be classified in four different categories. Flights classified in categories 1 and 3 (corresponding to RF7 and RF11 in Figure 2) had a changing supersaturation setpoint (three different values changing every 5 min throughout the flight). The uncertainty in supersaturation at each setpoint, however, is much higher for category 1 flights than for category 3 flights owing to a greater uncertainty in the sheath flow rate and/or column temperature gradient. Flights designated as category 1 also had a drifting pressure in the CCNc (except for RF7, where the entire flight was at constant altitude) causing shifts in supersaturation, while category 3 flights made use of the inlet pressure controller. The supersaturations for the category 3 flight shown (RF11) remain consistent throughout, even as the ambient pressure changes (except when pressure drops the pressure box control setting of 700 mbar). Even with the pressure control box, minor supersaturation deviations still exist owing to changes in ambient temperature. Categories 2 and 4 (represented by RF9 and RF19 in Figure 2) were set to a single supersaturation, but with pressure changes, and larger uncertainty in flow and temperature uncertainty in the former. Because the supersaturation was set to a constant value for the categories 2 and 4 flights, it is easier to see the effect of the abrupt change in the temperature setpoint as the ambient temperature changed inside the cabin of the aircraft.

[19] Although the variance of the calculated instrument supersaturation is low, *Rose et al.* [2008] suggest that the relative supersaturation uncertainty (at low supersaturations) can be as high as 10% owing to uncertainties in the parameters used to calibrate the instrument, such as water activity and nonspherical particle shape. We assume 10% as an upper limit of supersaturation uncertainty for categories 3 and 4 flights, and we assume an uncertainty in supersaturation of 20% for categories 1 and 2 flights. Instrument supersaturation uncertainty translates to uncertainty in the predicted CCN concentrations; for the levels cited here it could be important depending on the steepness of the CCN spectrum (which is a convolution of aerosol size distribution, composition and mixing state) at the supersaturation of

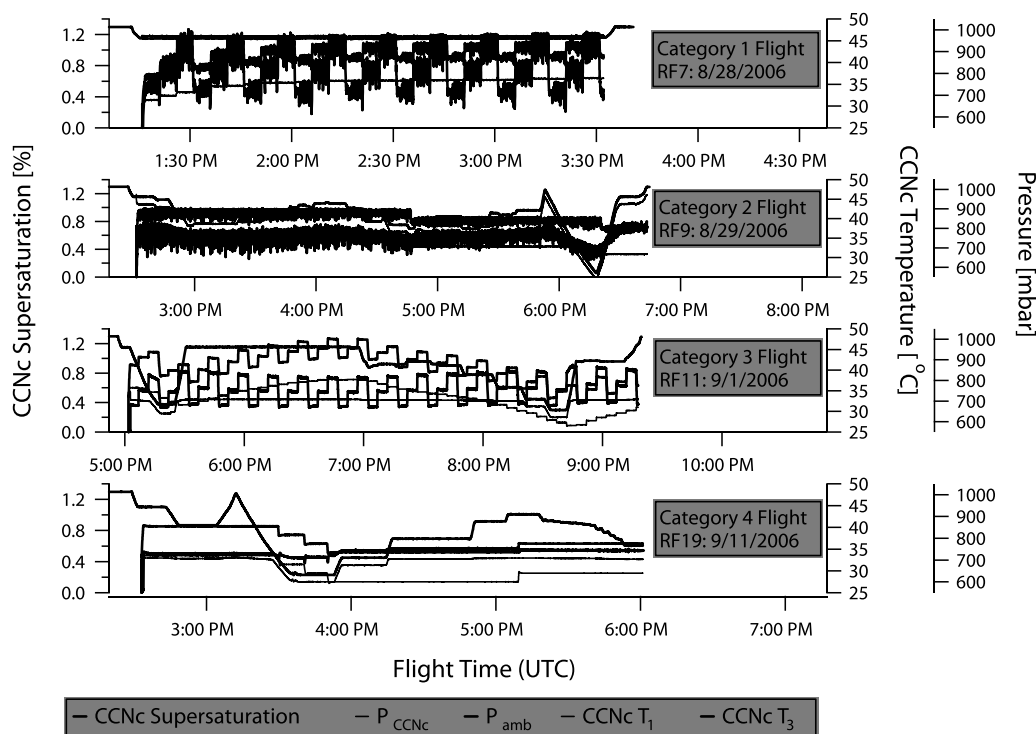


Figure 2. CCNc operating conditions (pressure, temperature, and supersaturation) for four representative flights.

interest. Although not straightforward, the sensitivity of CCN concentration to supersaturation uncertainty can be evaluated from the observed particle size distributions, given assumptions about the particle composition (section 2.4).

2.3. Measurements Used for CCN Closure

[20] Measurements used for CCN closure calculations (in addition to CCN concentrations) are dry particle size distributions (with relative humidity at $21\% \pm 5\%$, during all flights) measured by the Dual Automated Classified Aerosol Detector (DACAD [Wang *et al.*, 2003]), and the aerosol chemical composition measured by an Aerodyne Compact Time of Flight Aerosol Mass Spectrometer (C-ToF-AMS [Drewnick *et al.*, 2005; Sorooshian *et al.*, 2008a]). The CCNc and C-ToF-AMS were positioned on the same aerosol sampling manifold, which was switched between “counterflow virtual impactor in-cloud” and “main inlet out-of-cloud” modes. Since the DACAD sampled continuously from the main inlet, mobility size distribution measurements of cloud droplet residuals were not available, and therefore CCN closure cannot be evaluated for cloud droplet residuals. In computing the size distribution, we assume that particles measured in the DACAD are spherical, which is typically valid in a humid environment (even when the aerosol is dried appreciably), owing to depression of the efflorescence point by the organic compounds present in the particle [Salcedo, 2006; Chan *et al.*, 2008].

[21] An important temporal limitation is associated with the measurement of aerosol size distribution (73 s). For each scan, the average number concentration of CCN and supersaturation within the CCNc is computed. This data set is then filtered by disregarding 73-s segments of data when the

CCNc instrument supersaturation varies by 20% or more (from column temperature changes or pressure fluctuations during ascents/descents). To disregard aliasing biases from sampling smaller plumes that are below the temporal resolution of the DACAD, we filter out points for which the standard deviation of CCN exceeds 25% of the average CCN concentration. We further filter out data points when the average condensation nuclei (CN) concentrations differ by more than 50% from the total particle concentrations integrated from the measured DACAD size distribution.

[22] For the CCN closure analysis, we use bulk chemical composition from the C-ToF-AMS measurements, unless specified otherwise. Size-resolved AMS measurements have been used for several ground- and ship-based CCN closure studies [e.g., Medina *et al.*, 2007; Ervens *et al.*, 2007; Quinn *et al.*, 2008], where the air mass passes at a rate of 1 to 10 m s^{-1} . In airborne CCN closure studies, the airspeed is 10 to 100 times greater and air mass composition changes rapidly, requiring higher sensitivity and time resolution for the size-resolved composition measurements. While size-resolved measurements can be obtained rapidly in high-concentration plumes [e.g., Murphy *et al.*, 2009; Sorooshian *et al.*, 2008a], the loadings during many portions of the flights in this study were too low to obtain size-resolved composition in reasonably short time frames. As a result, size-resolved data was not used for CCN closure in this paper. However, the effect of size-resolved composition measurements is shown for specific cases where the signal-to-noise ratio for both the sulfate and organic size distributions is high.

[23] A Droplet Measurement Technologies integrated photoacoustic and nephelometer aerosol spectrometer

(PAS) was also operated onboard the CIRPAS Twin Otter. The PAS measures aerosol absorption and $\sim 5^\circ$ – 175° integrated scattering, using a laser radiation source, and an acoustic resonator coupled with a microphone to detect the photoacoustic signal from absorption. A Lambertian diffuser, mounted at the center of the acoustic resonator, is used to measure the light scattered by the aerosol. The standard laser installed by the manufacturer is a 781-nm solid state laser which failed under the high temperatures experienced in the aircraft cabin during some of the flights (a replacement 870-nm laser was then used for the rest of the campaign). The PAS collects data at a sampling rate of ~ 0.71 Hz. Zero air (cleaned of particles by means of a HEPA filter) data are automatically collected every 6 min to correct for background drifts. A thorough calibration of the PAS (with the 870-nm laser) was carried out at the end of the campaign in the laboratory using various concentrations of strongly and weakly absorbing particles. Altogether, the calibration procedure, instrumental noise and high-frequency changes in the background signals introduce an estimated 20–30% uncertainty in the absorption measurements discussed here. A PAS prototype, developed at the Desert Research Institute, Reno, Nevada, has been extensively tested and successfully deployed in past field campaigns [Arnott and Moosmüller, 1998; Arnott et al., 1999; Moosmüller et al., 1998; Arnott et al., 2006]. PAS observations are shown for one flight (using the 870-nm laser) to infer the impact of soot on CCN concentrations.

2.4. Prediction of CCN Concentrations

[24] To predict CCN concentrations from the measured size distribution (assuming that all particles have an internally mixed composition), we first determine the diameter of the smallest CCN-active particle (d_{50} ; where “50” signifies that a dry particle with this size has a 50% probability of activating into a cloud droplet) given the assumptions about internally mixed particle chemistry, using the following thermodynamic relationship [Seinfeld and Pandis, 2006]:

$$d_{50} = \left[\frac{27}{4} \left(\ln \left(\frac{S}{100} + 1 \right) \right)^2 \left(\frac{\rho_w TR}{4M_w \sigma} \right)^3 \frac{\rho_s M_w \varepsilon_s v}{M_s \rho_w} \right]^{-1/3}, \quad (2)$$

where S is the average instrument supersaturation (in %), T is the mean temperature within the CCNc column, R is the ideal gas constant, σ is the droplet surface tension at the point of activation, ρ is the density and M is molecular weight of the solute (subscript s) and of water (subscript w), and ε_s and v are the solute volume fraction and effective van't Hoff factor, respectively. Unless specified otherwise, the surface tension used in equation (2) to predict CCN concentrations is 69.9 mN m^{-1} , which is the surface tension of pure water at the average temperature of the observations. CCN predictions are calculated by summing all particles with diameters above d_{50} , accounting for fractional activation of the DACAD size bin containing d_{50} .

[25] For the flights where chemical composition information is used, we assume that the measured species are internally mixed. Furthermore, since the solubility of organics, their surfactant properties and mixing state are unknown, they are first treated as insoluble and nonsurfactant (the effect of these assumptions on CCN closure is

addressed with appropriate sensitivity studies). The organic volume fraction (ε_{org}) is then computed as

$$\varepsilon_{org} = (1 - \varepsilon_s) = \frac{m_{org}/\rho_{org}}{m_{org}/\rho_{org} + m_{AS}/\rho_{AS}}, \quad (3)$$

where m_{org} and m_{AS} are the mass loadings of organics and ammonium sulfate (the sum of ammonium and sulfate ions), respectively, obtained from the C-ToF-AMS, ρ_{AS} is the density of ammonium sulfate (1.76 g cm^{-3} [Hinds, 1999]) and ρ_{org} is an average density of organics, assumed to be 1.4 g cm^{-3} . The density of organics may range from 1.4 g cm^{-3} to more than 1.6 g cm^{-3} [Dinar et al., 2006]; we use the lower end of the organic density range to simulate the largest effect expected from internally mixed organics, as further explained in the following paragraph. When not including the bulk aerosol composition, we assume as a zero-order approximation that particles are composed of ammonium sulfate ($\varepsilon_s = 1.0$ in equation (2)). Following the guidance of Rose et al. [2008], v for ammonium sulfate (whether pure or internally mixed with organics) is set to 2.5.

[26] The two compositional assumptions presented above (pure ammonium sulfate versus internally mixed insoluble organic) represent limiting states of aerosol hygroscopicity. Ammonium sulfate is one of the most CCN-active and abundant compounds found in accumulation mode aerosol; assuming that the particles are composed purely of ammonium sulfate will thus tend to overestimate their CCN activity. Conversely, assuming organics are insoluble neglects their potentially important impacts on droplet activation, thereby leading to a tendency for underpredicting CCN number. In reality, we expect that the hygroscopicity of ambient particles lies somewhere between these two extremes. There are many other details about the aerosol composition that may affect the CCN closure (such as surfactant components, externally mixed particles, and size-varying composition), which are insufficiently constrained by the observations. We therefore first apply these two common assumptions to the whole data set to evaluate how well CCN closure can be attained. We then evaluate for specific cases the impact of more detailed composition information on CCN prediction accuracy.

[27] The uncertainty in predicted CCN concentration is influenced by uncertainties in the instrument supersaturation, particle size distribution and chemical composition. Assuming an internally mixed composition that is invariant with particle size, an estimate of CCN concentration sensitivity to supersaturation uncertainty can be obtained. For a period of very poor closure at ~ 1615 UTC on RF22, a 10% reduction of the instrument supersaturation causes a slight increase in d_{50} (from 46.4 nm to 53.0 nm), which decreases the predicted CCN concentrations from 1630 cm^{-3} to 1470 cm^{-3} . Given that the measured CCN concentrations are only 580 cm^{-3} during this time period, the uncertainty in predicted CCN concentrations clearly cannot explain the poor closure for this example.

3. Results

3.1. Summary of CCN Observations

[28] Table 1 summarizes the range of CCN concentration and supersaturation for all research flights during which the

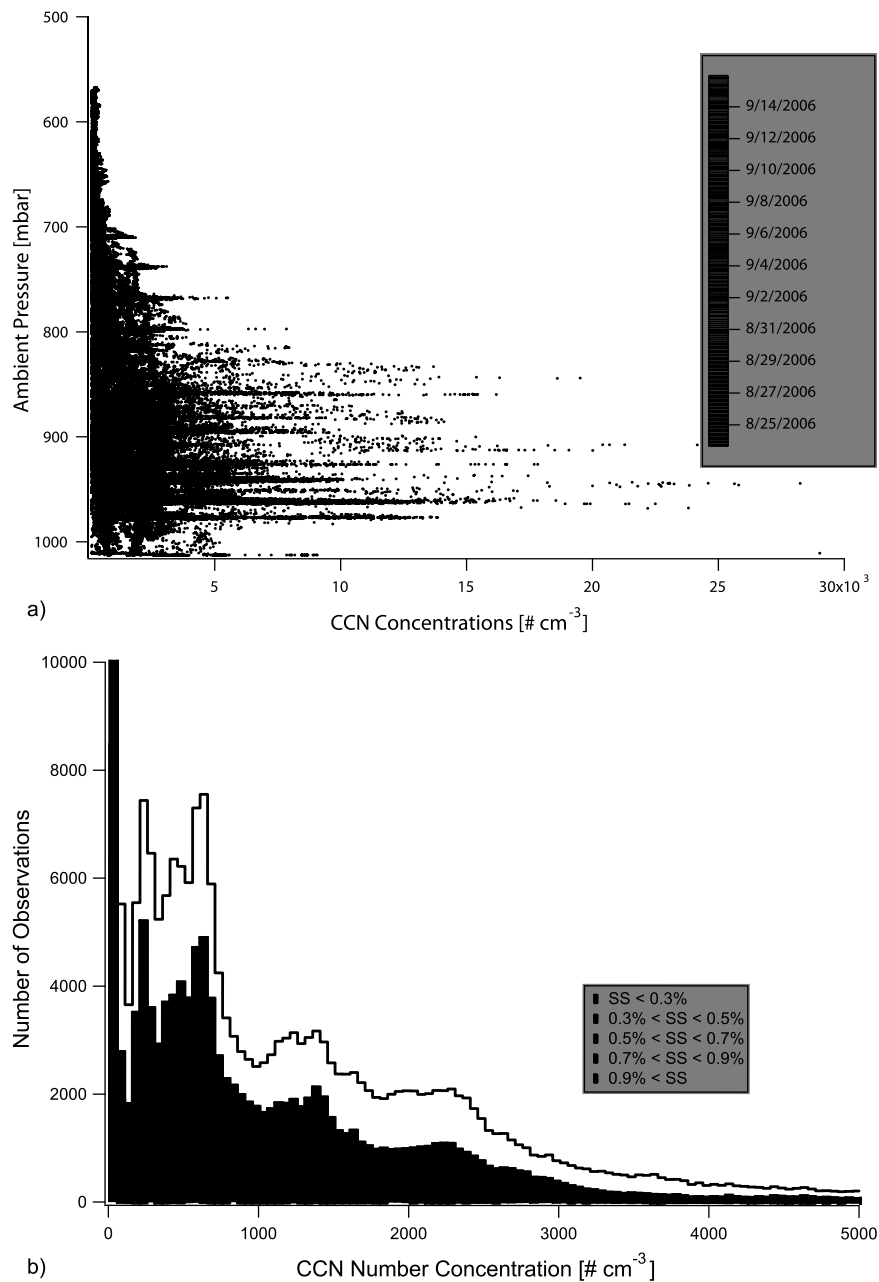


Figure 3. The 1-Hz CCN observations obtained during this study (a) plotted as a function of ambient pressure and time (exposed to a range of supersaturations, from 0.3% to 1.0%) and (b) expressed as a supersaturation range histogram. Total CCN are plotted as the solid black line in Figure 3b.

CCNc was operating. Figure 3a shows the profile of 1-Hz CCN data from the entire GoMACCS campaign as a function of ambient pressure, and colored by date. For many of the flights, CCN concentrations exceeded $10,000 \text{ cm}^{-3}$ (for a range of supersaturations, from 0.3 to 1.0%). On separate days, the CCN concentrations exceeded $20,000 \text{ cm}^{-3}$ (again, for a range of supersaturations, as low as 0.3%). Figure 3b shows the frequency distribution of CCN concentrations with different supersaturation ranges over the entire GoMACCS campaign. The solid line indicates the sum of the shaded regions, which is the total frequency distribution of CCN.

3.2. CCN Closure

[29] We first evaluate the extent to which CCN closure can be achieved using the measured size distribution and the assumption of pure ammonium sulfate particles. Figure 4a shows a summary of this simplified CCN closure colored by flight, for all the flights shown in Figure 1a. The gray lines indicate overprediction and underprediction by factors of 2, 3 and 4. Despite the very simple composition assumption, predictions are nearly always within a factor of 2 of the measurements. Figure 4b shows that the simplified CCN closure error is not correlated with supersaturation, but rather with particle concentration. The overprediction

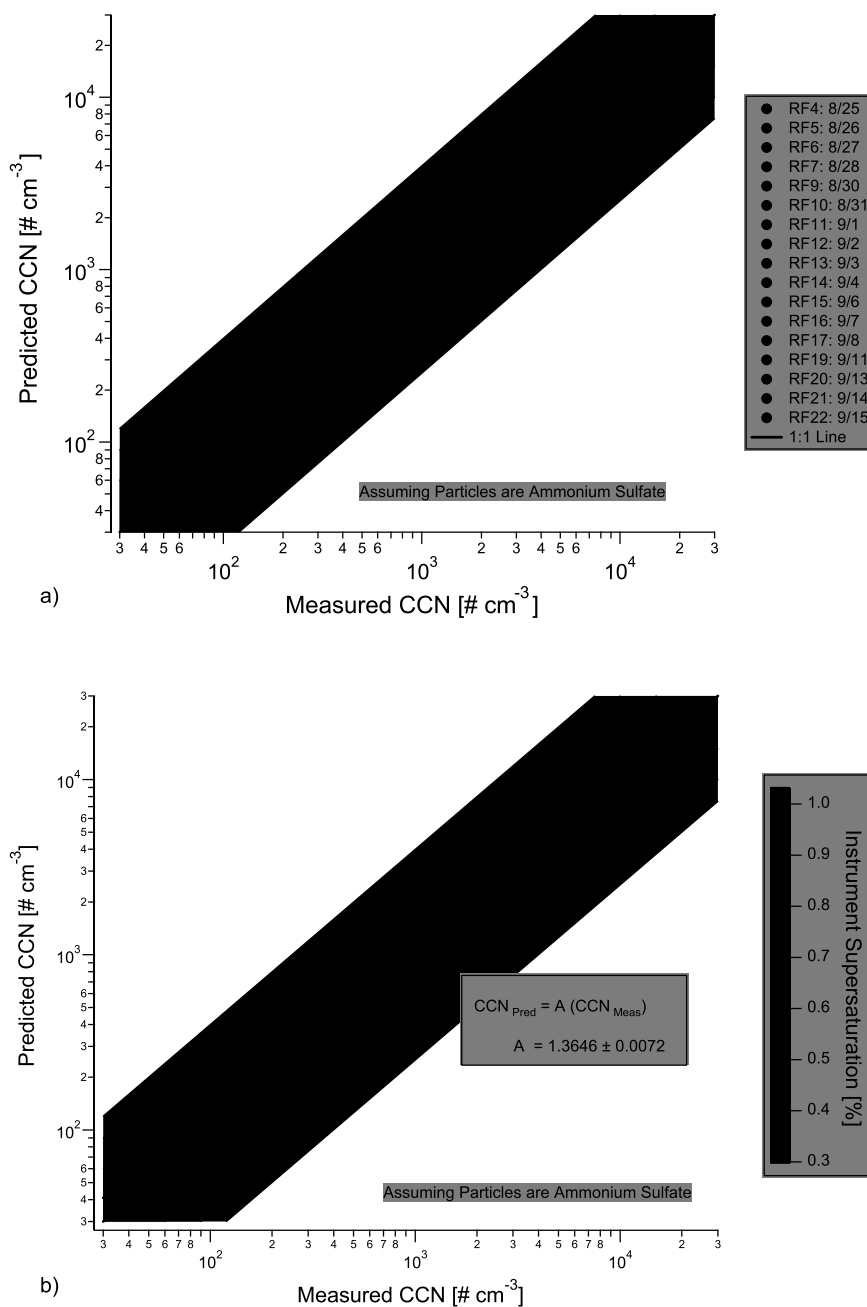


Figure 4. CCN closure for all flights, assuming pure ammonium sulfate aerosol. The thick solid line shows the 1:1 relationship, and the gray bands indicate overprediction and underprediction by factors of 2–4. Symbols are colored with respect to (a) research flight number and (b) instrument supersaturation. The dashed line in Figure 4b shows the best fit relationship with the given equation.

(~36%) is constant for CCN concentrations ranging from 1,000 to 10,000 cm^{-3} . At lower CCN concentrations (suggestive of a cleaner air mass), the bias is lower. At the highest concentrations (above 10,000 cm^{-3}), the overprediction bias decreases again. Since there is no clear dependence of the CCN overprediction on instrument supersaturation and CCN concentration, water vapor depletion in the CCNc is unlikely the cause for the CCN overprediction observed (laboratory experiments further support this, as they have shown that water vapor depletion does not reduce the maximum supersaturation in the CCNc for CCN

concentrations up to at least 10,000 cm^{-3}). Instead, the composition of the aerosol population is expected to play a role.

3.3. CCN Closure With Chemical Analysis

[30] Figure 5 shows the CCN closure for all flights to which bulk aerosol chemical composition from C-ToF-AMS data is applied. In both Figures 5a and 5b, the colored data points correspond to CCN closure calculations assuming that organics are internally mixed with sulfate for all particles. Figure 5a shows the CCN closure colored by flight

concentrations; this representation of the CCN closure prevents the higher CCN concentration observations from controlling the fit. The result is a more modest improvement in CCN closure from the inclusion of bulk chemical information (with a decrease in the CCN overprediction bias from 34% to 20% using the ratio method, as opposed to a decrease from 36% to 3% using the linear fit). Furthermore, using the ratio method, the standard deviation decreases slightly from 24% to 19% when including the bulk chemical information (which is a more significant change than that of the linear regression coefficients). Overall, these results are consistent with studies published to date [e.g., *Medina et al.*, 2007; *Chang et al.*, 2007; *Wang et al.*, 2008; *Ervens et al.*, 2007], which show that CCN concentrations can be more accurately predicted assuming that the measured organics are insoluble.

[31] Organics can also lower the surface tension of deliquesced CCN, facilitating activation (potentially making the particles even more CCN-active than ammonium sulfate [*Asa-Awuku et al.*, 2008]). Figure 5a presents the impact of reducing surface tension by 15 mN m^{-1} on CCN closure (gray pluses), using the same composition information as the colored data points. This degree of surface tension reduction is typical for organic-rich ambient particles [e.g., *Facchini et al.*, 2000; *Decesari et al.*, 2005; *Mircea et al.*, 2005; *Asa-Awuku et al.*, 2008]. The modest surface tension depression may reconcile the CCN underprediction bias, even for cases where the aerosol is mostly composed of ammonium sulfate.

[32] Although simply adding the assumed internally mixed organic fraction to the CCN closure analysis reduces the overprediction bias, it cannot be established if the improved CCN closure occurs for the right reasons. It may be hypothesized that the CCN overprediction bias is controlled by the internally mixed aerosol composition (as measured by the C-ToF-AMS), whereas the variability in the CCN closure is governed by the externally mixed hydrophobic fraction (assuming that a significant fraction of the externally mixed hydrophobic aerosol mass is undetected by the C-ToF-AMS, such as soot and dust); this would be consistent with the reduced bias resulting from the internally mixed assumption without a large reduction in the variability (since the mixing state is unknown). Without particle-by-particle information or measurements of the aerosol mixing state, it is not possible to verify this hypothesis. Hygroscopicity measurements (especially with high temporal resolution, e.g., the differential aerosol sizing and hygroscopicity spectrometer probe [*Sorooshian et al.*, 2008b]), or single-particle mass spectra measurements in the size range 40–200 nm, may be needed to adequately address the affect of aerosol composition on CCN closure.

[33] In sections 3.4 and 3.5, we examine specific flights and the CCN closure in relation to specific aerosol sources, in an attempt to evaluate the chemical factors influencing the observed CCN concentrations.

3.4. Research Flight 7 (28 August 2006)

[34] During RF7, back trajectories computed with the Flexpart model (<http://zardozi.nilu.no/~andreas/TEXAQS/>) suggest the wind blew consistently out of the Gulf of Mexico and then curved toward the northeast over the city of Houston. The consistent meteorology provided an op-

portunity to examine the evolution of emissions from specific chemical plants and refineries along the Houston Ship Channel as the emissions traveled downwind. Figure 6a shows the flight track for RF7, colored by the time of day, first starting at Ellington Field southeast of downtown Houston, followed by transects of the Houston plume downwind, then followed by approaches toward and away from specific point sources previously identified. The plumes identified by particle concentrations in excess of $10,000 \text{ cm}^{-3}$ (colored in gray) appear to be correlated with specific point sources identified in the 2004 EPA NO_x emission inventory. Figure 6b presents the flight track colored by the organic volume fraction (calculated from equation (3)), which ranges between 0 and 0.3 for this flight, with the higher values at roughly the same locations as those of elevated particle concentrations. The maps (Figures 6a and 6b) also show the location of the Houston city limit, major roadways and airports, the Houston Ship Channel, and several of the largest point sources for NO_x , including petrochemical refineries (Ref), chemical plants (Chem P) and power plants (PP).

[35] Figure 7a shows the time series of all the measurements relevant for CCN closure including the distribution of dry particle size (d_p), the C-ToF-AMS measured aerosol chemical composition and the CCNc supersaturation (blue bars). Also shown are the average measured (open circles) and predicted (solid circles) CCN concentrations assuming that the particles are composed of (1) pure ammonium sulfate (blue), and, (2) a size-independent internal mixture of insoluble organics and ammonium sulfate (orange), filtered by supersaturation and concentration fluctuations and discrepancies as described earlier in the text. Particle concentrations above 10 nm measured with a TSI 3010 condensation nuclei counter are plotted (gray line) along with particle concentrations integrated from the particle size distribution measurements (blue horizontal lines). The pressure trace (black line) indicates that the whole flight occurred at a single low altitude. At the top of Figure 7a, the distribution of droplet size (D_p) is shown, which clearly shows the effect of changing supersaturation on the droplet size at the exit of the CCNc.

[36] The particle concentration spikes observed in the first half of the flight correspond to plume transects. Starting around 1430 UTC, the in-plume legs began. Two sections are highlighted with blue and pink shaded areas in Figure 7a and correspond to when the Twin Otter first flew from and toward two point sources along the Houston Ship Channel; Figure 7b presents these sections in higher resolution. The blue shaded area corresponds to the plume labeled “1” in Figure 6a while the pink shaded area corresponds to plume “2.” For both plumes, the overprediction is greater when sampling closer to the point source, and cannot be attributed to the specific internally mixed composition assumption (since the blue and the orange points lie almost on top of each other, consistent with the low-volume fraction of organics for this flight). Thus, we expect that the overprediction originates from unresolved mixing state and composition variation with size. The improvement in CCN closure further from specific point sources may imply that the aerosol composition changes rapidly downwind of the aerosol source. However, the CCNc supersaturation was also coincidentally higher as we sampled nearer to the point

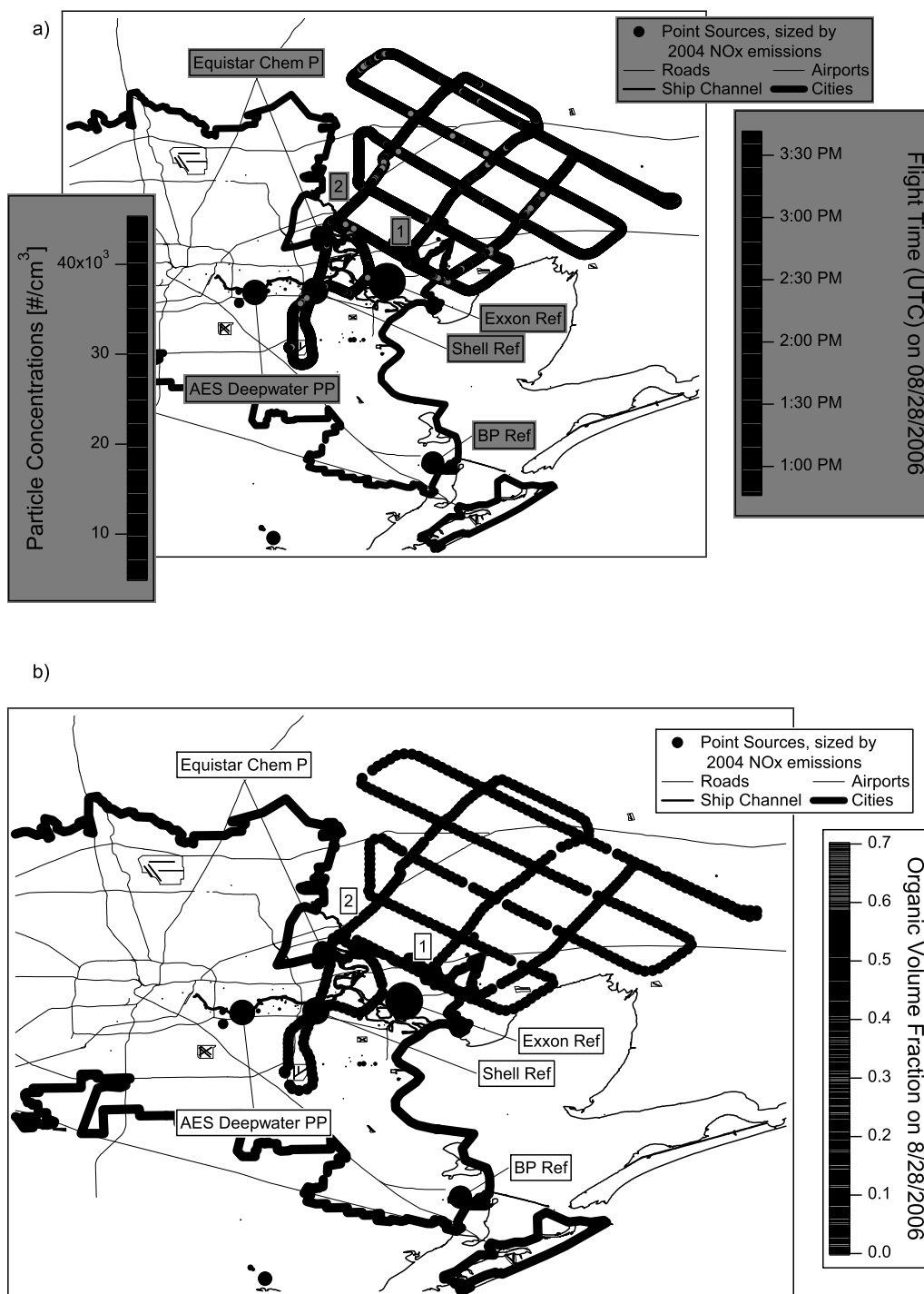
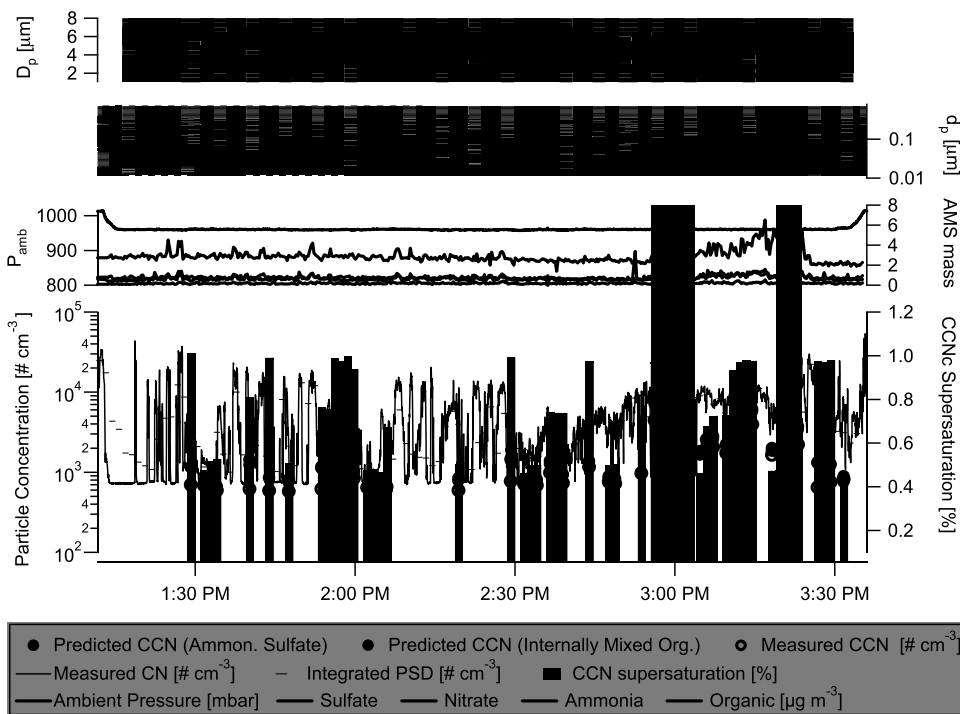


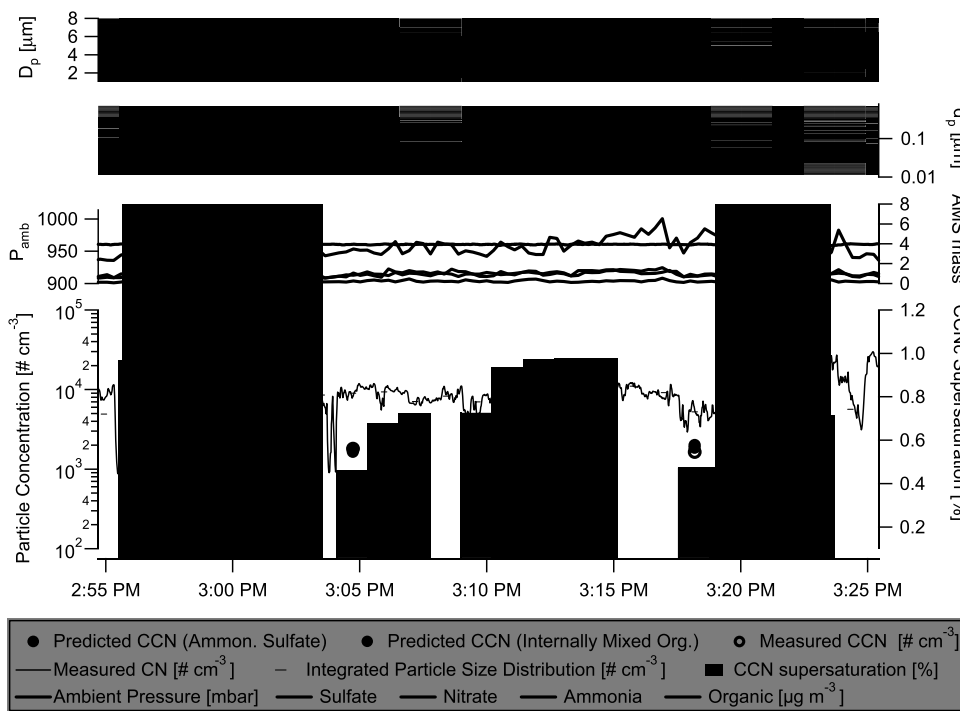
Figure 6. Flight track for RF7. Aircraft position colored by (a) flight time, where sections with particle concentrations (with diameter larger than 10 nm) greater than $10,000 \text{ cm}^{-3}$ are shown in grayscale, and (b) aerosol organic volume fraction (calculated as explained in the text). Map scale is approximately 80 km across.

sources for these two cases. It may be that the CCN closure is improved at low supersaturations (corresponding to a larger d_{50}) because most of the CCN are internally mixed, whereas at higher supersaturations (corresponding to a smaller d_{50}) there are more externally mixed particles. Since the aerosol mass is weighted strongly by the particle size, another possibility is that the bulk aerosol composition

measured by the C-ToF-AMS does not adequately represent the smaller particles, which could then have a higher organic mass fraction and act less efficiently as CCN. For most of this flight, the size-resolved C-ToF-AMS measurements were unable to show conclusively whether the size distribution of organics is different from the sulfate size



a)



b)

Figure 7. Time series for RF7 of measured and predicted CCN concentrations, particle concentrations with $d_p > 10$ nm, ambient pressure and AMS measured mass loadings of sulfate, organic, nitrate, and ammonium ions. Results shown (a) for the whole flight and (b) for data collected between 1455 and 1523 UTC. At the top of Figures 7a and 7b are image plots of dry particle diameter (d_p) and droplet diameter (D_p) size distributions, colored by the bin-normalized concentrations (colorbar not shown). The CCNc supersaturation is plotted as bars. Blue and pink shaded areas depict regions of interest, as described in the text.

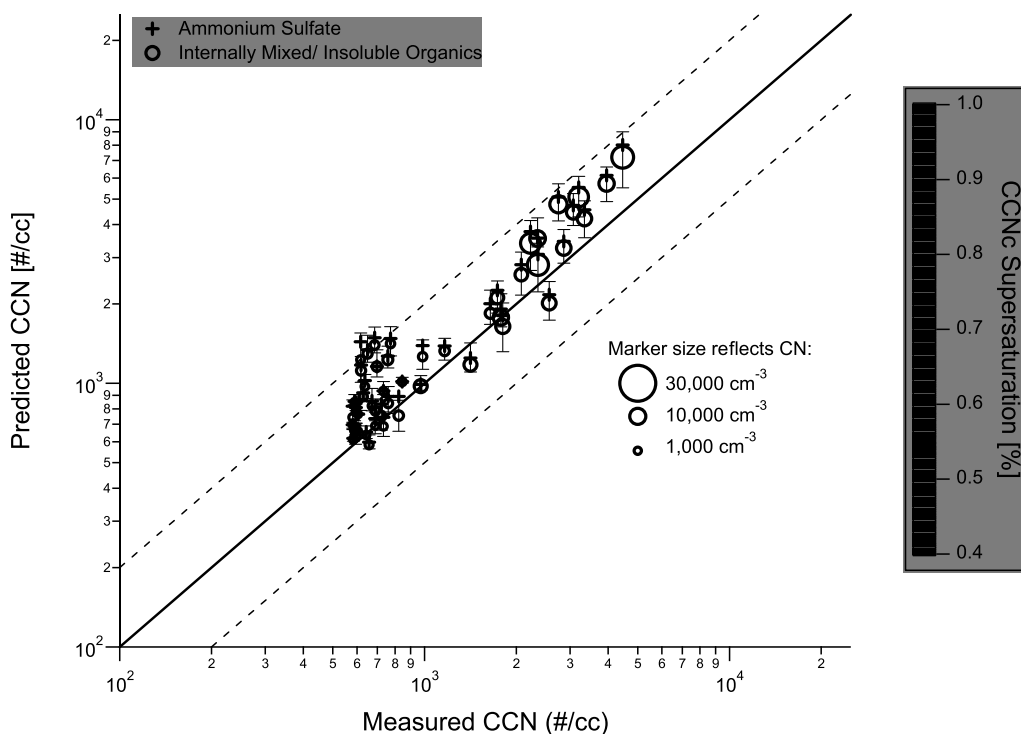


Figure 8. CCN closure for RF7 with different assumptions about particle chemistry. Colors represent the CCNc supersaturation, and marker size reflects the ambient particle concentrations. Vertical error bars are based on a supersaturation uncertainty of 20%. Dashed lines indicate underprediction and overprediction by 100%.

distribution (which could then be used as evidence for an externally mixed aerosol), since the organic mass loadings were quite low (average for flight = $0.65 \pm 0.26 \mu\text{g m}^{-3}$).

[37] Figure 8 shows that the CCN closure for the duration of RF7 is much better at lower supersaturations. The color of the open circles indicates the CCNc supersaturation, while the size of the markers is proportional to the concentration of particles. The vertical error bars represent the effect of a 20% uncertainty in the instrument supersaturation, assuming an internally mixed composition. *Ervens et al.* [2007] also found a supersaturation-dependent overprediction bias for CCN closure at Chebogue Point, Nova Scotia, attributed to undercounting in the CCNc from using a higher than recommended flow rate in the CCNc. An even higher flow rate is used in this study; however, the observed droplet size distribution in Figure 7b shows that the particles are all above $2 \mu\text{m}$ (hence efficiently counted), demonstrating that the flow rate recommendations for prevention of undercounting in the CCNc suggested by *Lance et al.* [2006] are conservative. Furthermore, in this study, CCN closure was better at low supersaturations, opposite to what was seen by *Ervens et al.* [2007]. Thus, size-varying composition (and not instrument artifacts) is likely responsible for the trend in CCN prediction bias with supersaturation.

3.5. Research Flight 22 (15 September 2006)

[38] We now examine data from a flight in which sampling was carried out farther from emission sources. During RF22, back trajectories computed with the Flexpart model suggest a prevailing wind originating from the Gulf of Mexico and flowing northwest over Houston; closer anal-

ysis of the trajectories (not shown) suggest the wind direction changed throughout the flight, at times picking up biomass burning emissions from central Texas and Louisiana. Figure 9a shows the flight track for RF22 (with marker size reflecting the ambient pressure, and color, the time of day); the Twin Otter first flew along the highly industrialized ship channel, followed by a low-pass over downtown Houston and several transects of the Houston plume downwind of the city. Marked on the flight track are segments where particle concentrations exceed $10,000 \text{ cm}^{-3}$ (indicating the regions of highest concentrations), which occur inside the city of Houston and downwind thereof. Figure 9b is similar to Figure 9a, but colored by the organic volume fraction, which varies between 10% and 70% (much higher than in RF7). Figure 9b shows that the organic fraction is higher downwind of Houston; the 2004 emission inventory does not show any large sources for primary organic aerosol in this region, hence the organic fraction increase may be associated with secondary photochemical production from urban precursor emissions or mixing of regional biomass burning aerosol from central Texas. The fact that the location of high organics is intersected at least three different times between 1900 and 2000 UTC suggests a persistent feature consistent with the dominant wind direction.

[39] Similar to Figure 7, Figure 10 shows the time series during RF22 of measured and predicted CCN concentrations for two particle chemical composition assumptions, the measured aerosol size distribution, and, the measured particle composition. Compared to RF7, the aerosol mass and organic volume fraction in RF22 is substantially higher.

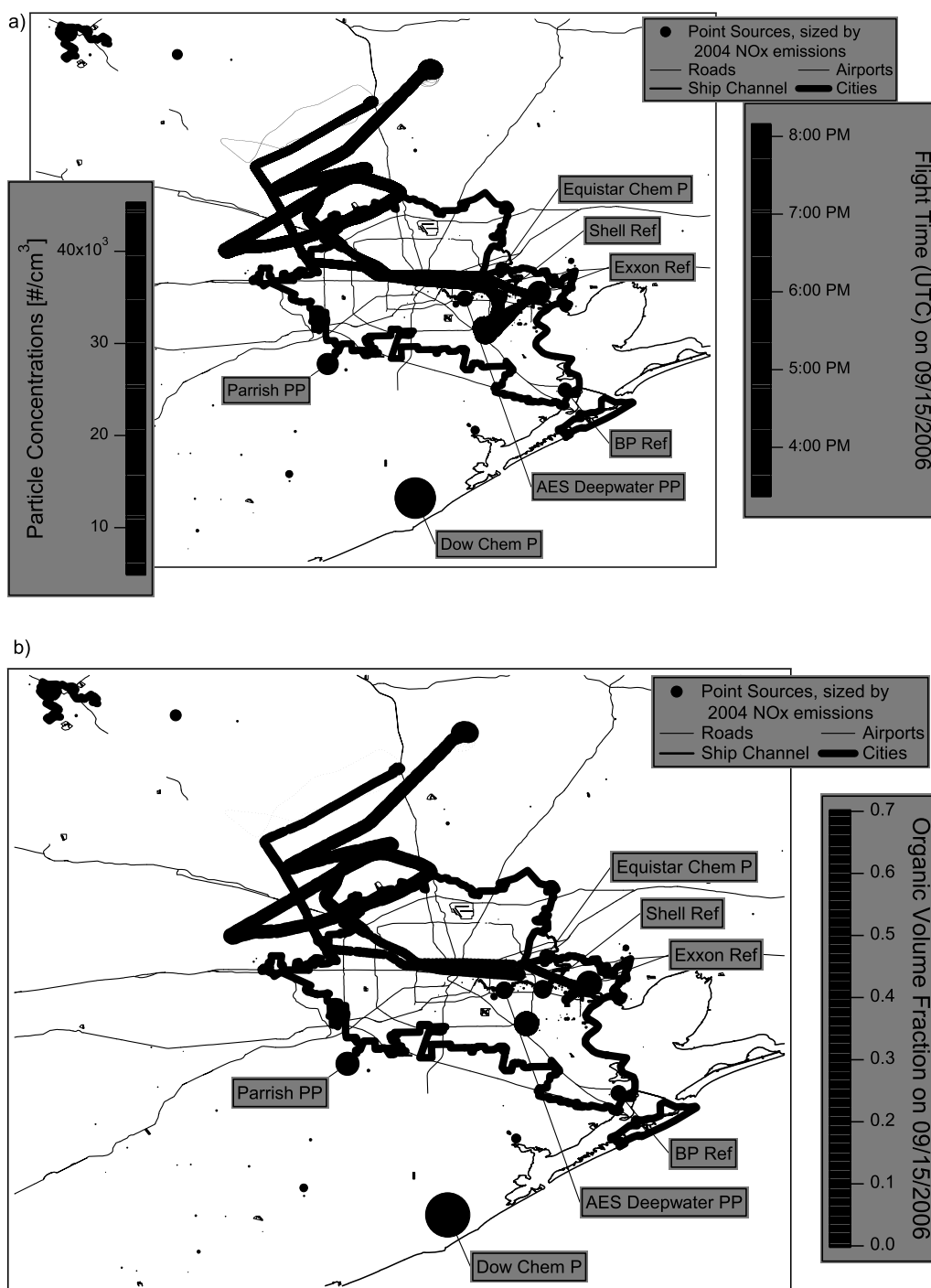


Figure 9. Flight track for RF22. (a) Aircraft position colored by flight time, with line thickness proportional to the ambient pressure (lower altitude legs have a thicker line); sections where particle concentrations (with diameter larger than 10 nm) are greater than 10,000 cm⁻³ are shown in grayscale. (b) Aircraft position colored by organic volume fraction, calculated as described in the text. Map scale is approximately 80 km across.

Figure 10 also presents an estimate of soot mass based on the photoacoustic absorption measurements. For this, the absorption coefficient (Mm^{-1}) is divided by the mass-absorption efficiency ($2.33 m^2 g^{-1}$ at 870 nm) extrapolated from a relation from Moosmüller *et al.* [1998], assuming that all absorbing material is externally mixed soot. This approach in general provides only an approximate estimate

of the soot mass since (1) absorption can be enhanced when internally mixed with nonabsorbing compounds [e.g., Mikhailov *et al.*, 2006], (2) coating can result in soot fractal aggregate collapse reducing the absorption, (3) the absorption efficiency has substantial uncertainty, and (4) other compounds in the aerosol beside soot (e.g., dust) can be absorbing. However, measurements from a single particle

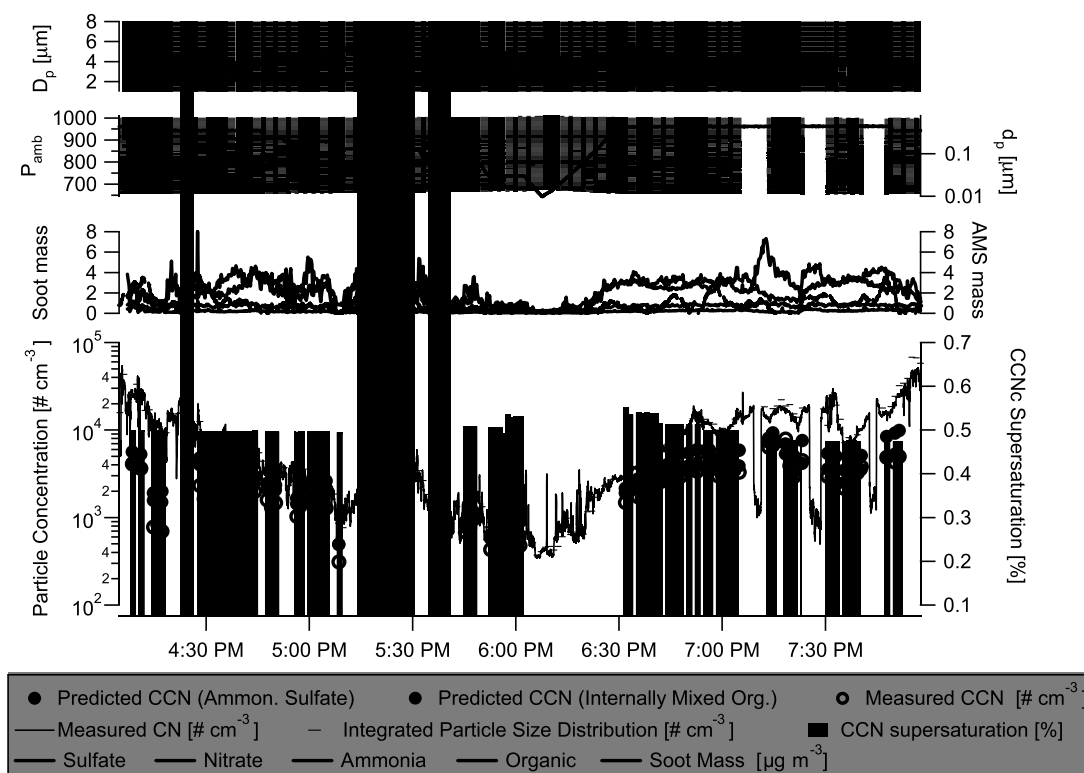


Figure 10. Time series for RF22 of measured and predicted CCN concentrations, particle concentrations with $d_p > 10$ nm, ambient pressure, and AMS measured mass loadings of sulfate, organic, nitrate, and ammonium ions. Also shown is the soot mass estimated from the photoacoustic absorption measurements. At the top are image plots of dry particle diameter (d_p) and droplet diameter (D_p) size distributions, colored by the bin-normalized concentrations (colorbar not shown). The CCNc supersaturation is plotted as bars. Vertical gray bars indicate time periods when the counterflow virtual impactor was turned on.

soot photometer during the concurrent TexAQS campaign suggest soot loadings as high as $2 \mu\text{g m}^{-3}$ in the Houston plume and a mixing state that is strongly external [Schwarz *et al.*, 2008]. The urban soot particles observed during TexAQS also show a size distribution centered around 60 nm [Schwarz *et al.*, 2008], which is very close to the average d_{50} we calculate for the particles during GoMACCS. Altogether, this suggests that a significant fraction of particles may be externally mixed soot that would not readily act as CCN.

[40] Figure 11 shows the particle size distribution during a period of very poor CCN closure (1630 cm^{-3} predicted CCN, and only 630 cm^{-3} measured CCN) on RF22 at 1614–1618 UTC. Using the photoacoustic absorption measurement to estimate the soot mass concentration as explained previously ($0.7 \mu\text{g m}^{-3}$ for this time period), and assuming that the local maximum in the particle size distribution at 65 nm is due to an external mixture of soot (consistent with the TexAQS observations), we infer a lognormal distribution of soot particles (with geometric standard deviation of 1.2). Assuming that this soot distribution does not contribute CCN, predicted CCN concentration drops to 720 cm^{-3} , which is only a 14% overprediction (as opposed to an almost 160% overprediction when assuming an internal mixture without any contribution from soot). An internal mixture of soot with the other aerosol species could also decrease the number of predicted CCN by reducing ε_s

in the particles (i.e., increasing d_{50}). However, to explain the observed CCN concentration, ε_s would need to decrease from 0.57 to 0.09 (i.e., an increase in d_{50} from 50.8 nm to 94.6 nm), which is not consistent with the composition measurements (with $\sim 1 \mu\text{g m}^{-3}$ sulfate and $0.8 \mu\text{g m}^{-3}$ organics measured by the C-ToF-AMS at that time, a lower estimate for ε_s would be ~ 0.38 , assuming a soot density of 2 g cm^{-3} [Slowik *et al.*, 2004]). Since soot aerosol in Houston was found to be most often externally mixed by Schwarz *et al.* [2008], and since the photoacoustic observations onboard the Twin Otter show significant absorption consistent with a large soot number concentration, we are confident that an external mixture of nonhygroscopic soot aerosol is contributing to the extreme CCN overprediction for this example. As the Twin Otter was sampling directly downwind of the Houston Ship Channel during that time, an external mixture with soot is not unexpected. However, when looking at Figure 10, there are clearly times when absorption is even higher, and yet the CCN closure is good (for example, at 1608–1611 UTC); this may result from the fact that the absorption measurements do not provide the mixing state or size distribution of the particle composition and the fact that other compounds such as dust can also contribute to the observed absorption.

[41] Owing to the high mass loadings of both organics and sulfate for much of RF22, the size-resolved particle composition measurements may also provide important

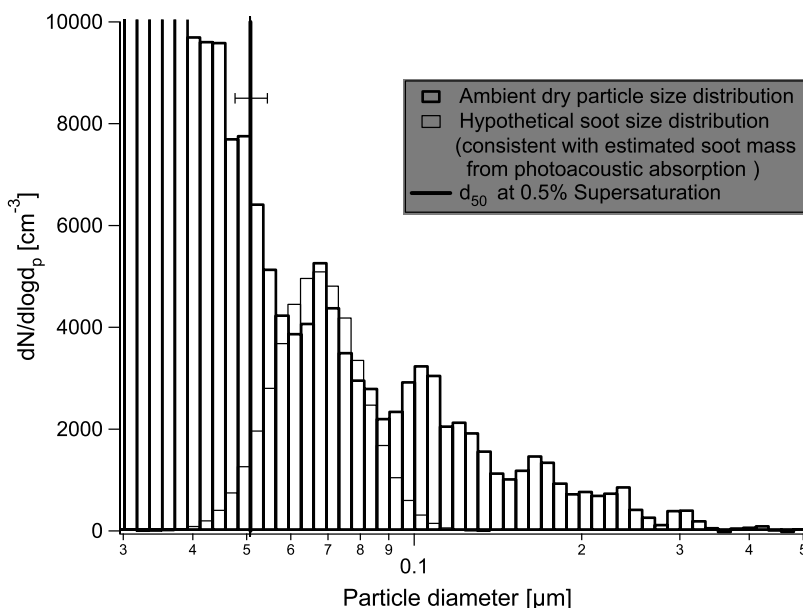


Figure 11. Particle size distribution (red bars) during a period of very high CCN overprediction on RF22 (at 1610–1618 UTC). Soot size distribution (blue bars) assuming a lognormal distribution with mean diameter of 65 nm, with particle number concentration constrained using estimated soot mass concentrations from photoacoustic absorption measurements. Vertical solid line indicates the smallest particle size expected to activate, d_{50} , given the assumptions of internally mixed aerosol composition. The horizontal error bar shows the effect of a 10% supersaturation uncertainty on d_{50} under the same assumptions.

insight for this flight. Figure 12a shows the size-resolved C-ToF-AMS measurements for the period of poor closure (160% CCN overprediction) at 1614–1617 UTC on RF22. These measurements, although noisy, confirm that the organic mass (like the soot mass) is likely externally mixed with sulfate since the size distributions of organic and sulfate mass are quite dissimilar. During another period of

poor closure on RF22 (76% CCN overprediction) at 1647–1650 UTC, the bulk of the sulfate and organic mass follow similar size distributions (Figure 12b) and the assumption of an internal mixture appears to be reasonable (at least for particles larger than about 200 nm). In addition, the expected soot mass during this time period is very low (the absorption is just above the detection limit of the

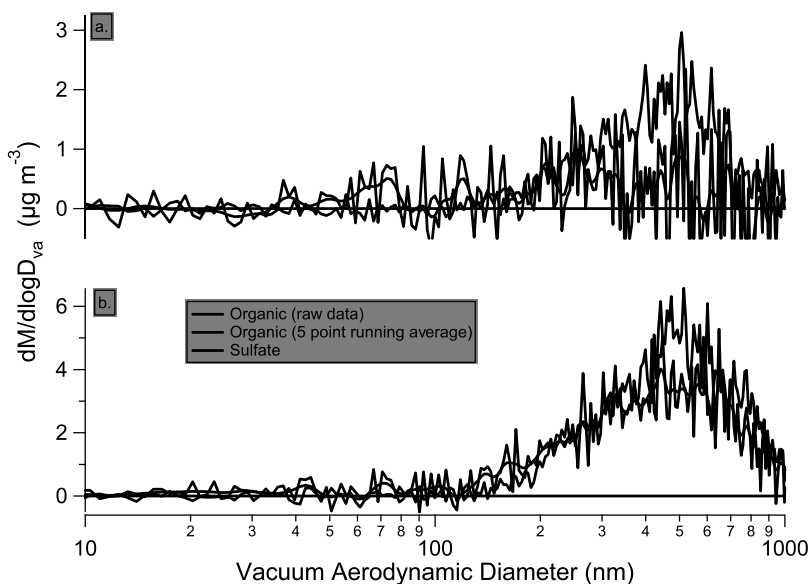


Figure 12. Size-resolved chemical composition measured by the C-TOF-AMS during RF22 at (a) 1614–1618 UTC (160% CCN overprediction) and (b) 1647–1650 UTC (76% CCN overprediction); $dM/d\log D_{va}$ is the observed mass for each size bin normalized by the bin width (in log space) of vacuum aerodynamic diameter.

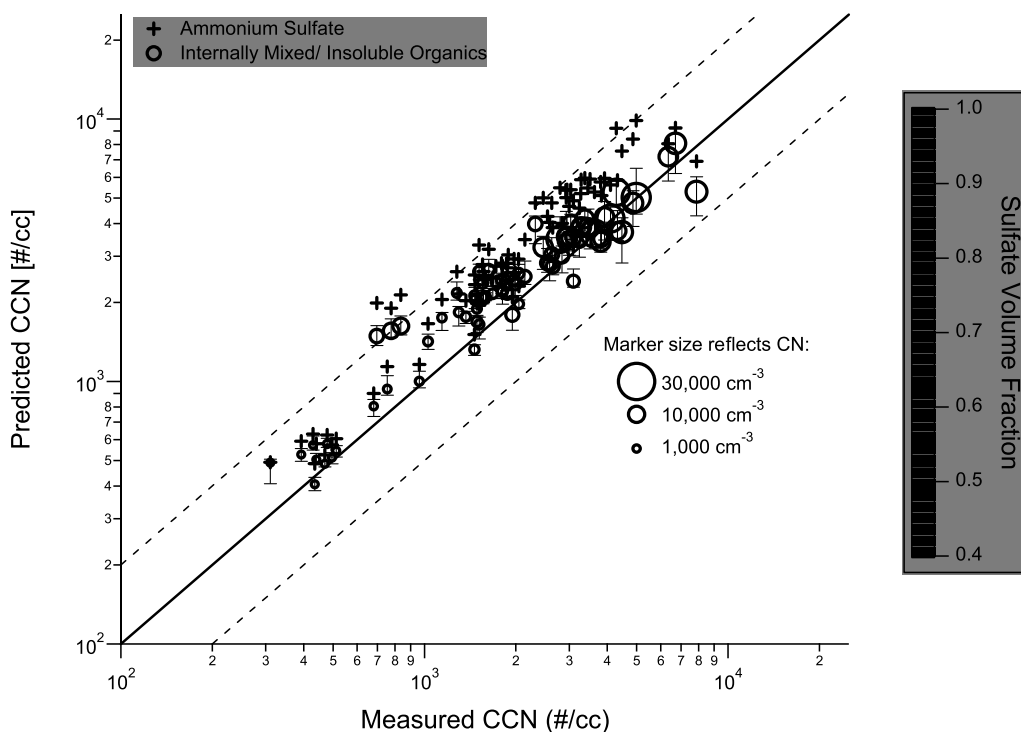


Figure 13. CCN closure for RF22 with different assumptions for particle composition. Higher organic volume fractions (represented by redder markers) are correlated with higher CCN and particle concentrations. Vertical error bars are based on a supersaturation uncertainty of 10%. Dashed lines indicate underprediction and overprediction by 100%.

photoacoustic measurements). Both time periods shown in Figure 12 have similar bulk organic to sulfate ratios (0.74 ± 0.12 for the period in Figure 12a and 0.87 ± 0.16 for the period in Figure 12b). However, the CCN overprediction is much lower for the second time period, and the mechanisms responsible for CCN overprediction may be different. Since the aerosol appears to be internally mixed, perhaps the effect of size-varying composition is controlling the CCN overprediction for the second time period. For particles smaller than about 200 nm (where many of the CCN occur), the ratio of organics to sulfate appears to be much higher than for particles larger than 200 nm (where most of the mass occurs); therefore, the soluble volume fraction derived from bulk composition may be biased high for the majority of particles smaller than 200 nm. In order to explain the number of observed CCN, the smaller particles (<200 nm) would need to be highly enriched in organics. The other possibility is that the smaller particles are much more externally mixed, which is not unexpected since many primary aerosol emission sources produce fine particulates. Unfortunately, it is not possible to unambiguously verify the extent to which either of these mechanisms is affecting the CCN closure, since the signal-to-noise ratio of the size-resolved C-TOF-AMS measurements at CCN relevant sizes (between about 50 to 200 nm) is very low.

[42] The CCN closure for RF22 is shown in Figure 13, where vertical error bars represent the effect of a 10% uncertainty in the instrument supersaturation on an internally mixed aerosol population. Figure 13 shows that CCN are, on average, overpredicted when assuming pure ammonium sulfate aerosol (not always by the same amount). On

average, the closure is not better than for RF7, although the uncertainty in the CCNc supersaturation is certainly lower. CCN closure improves when assuming that the measured bulk organic fraction is insoluble and internally mixed with sulfate. Under more polluted conditions (higher particle concentrations), assuming the organic fraction is internally mixed results in CCN underprediction; this suggests that the organics are either partially soluble or they depress droplet surface tension (thereby facilitating droplet activation and increasing CCN concentrations).

[43] The CCN closure calculations carried out here suggest that detailed knowledge of the particle chemical composition distribution (e.g., size-resolved chemical composition, surfactant properties and mixing state) are important for successful CCN closure in close proximity to heterogeneous emission sources such as those found in Houston, in agreement with the conclusions of *Cubison et al.* [2008].

3.6. Kinetics of Droplet Growth

[44] Figure 14 shows the average droplet diameter at the exit of the CCNc column for all flights as a function of the CCNc supersaturation. For comparison, we show the average droplet diameter for classified ammonium sulfate particles exposed to a range of supersaturations in the laboratory at 1 L min^{-1} total flow rate (dashed line in Figure 14). We vary the dry ammonium sulfate particle size from 10 nm to over 200 nm during the calibration to obtain the range of droplet sizes expected for a given supersaturation (gray shaded region in Figure 14). On average, the droplet diameter from ambient measurements is above the lower limit established by the calibration aerosol. Since

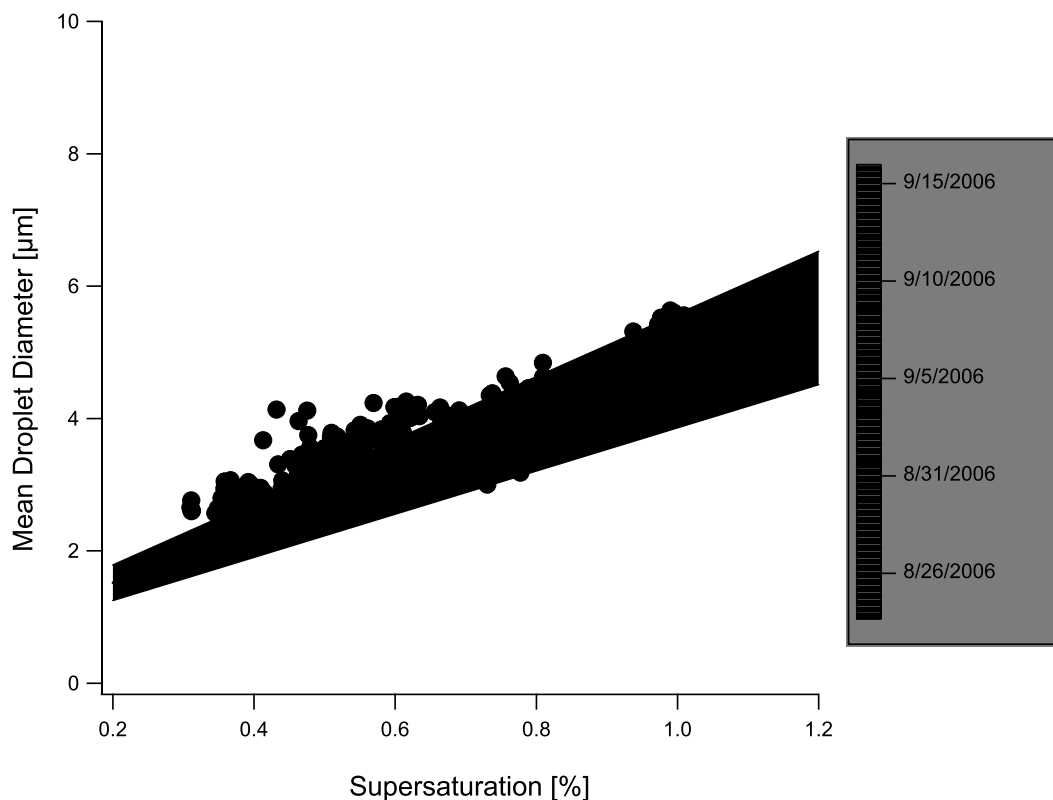


Figure 14. Average droplet diameter at the exit of the CCNc as a function of the instrument supersaturation for all ambient CCN measurements during the campaign. The gray shaded area indicates 1 standard deviation of the calibrations with ammonium sulfate aerosol.

the critical supersaturation of the ambient particles is unknown, the droplet size cannot be unambiguously related to the growth rate. The droplet growth rate is driven by the difference between the instrument supersaturation and the particle equilibrium supersaturation, and is also proportional to the amount of time the droplets are given to grow upon activation. Particles that activate at a lower supersaturation than the instrument supersaturation will have both a higher driving force for condensational growth and more time to grow (as they will activate even before supersaturation has fully developed in the instrument). Another factor influencing the droplet growth rate is the number of CCN present in the column, which can deplete the water vapor at very high particle concentrations. The ammonium sulfate calibrations supplied no greater than 600 cm^{-3} CCN at any given time; therefore, we expect that comparisons with ambient measurements having much higher CCN concentrations (and, therefore, potentially smaller droplet sizes) may affect our assessment of the droplet growth rate. However, Figure 13 supports that all droplets formed from ambient aerosol are, on average, larger than the droplet formed from calibration aerosol. This comparison, termed “threshold droplet growth analysis,” suggests that significant water vapor depletion does not occur within the CCNc, even with CCN concentrations up to $10,000 \text{ cm}^{-3}$. Furthermore, droplets on average do not grow more slowly than activated ammonium sulfate particles, which suggests that the presence of organics, for the range of supersaturations considered, does not substantially delay the activation kinetics of CCN. This is

contrary to the findings of *Ruehl et al.* [2008] who report up to 62% of the particles having moderate kinetic inhibition to condensational growth at a ground-based site in Houston during GoMACCS, using a phase Doppler interferometer to monitor the droplet size in another continuous-flow stream-wise thermal gradient CCN chamber. The apparent discrepancy between this study and *Ruehl et al.* [2008] motivates future side-by-side comparisons of the instruments to establish whether observed differences arise from differences in sampled particle phase state, or artifacts from the optical detection or thermal processing of the aerosol in either of the instruments [*Asa-Awuku et al.*, 2009].

4. Conclusions

[45] This study provides an airborne CCN closure analysis in a heavily polluted environment. Average CCN concentrations ranged from 100 cm^{-3} to more than $10,000 \text{ cm}^{-3}$, and organic volume fraction in the aerosol were as high as 70%. The results show that CCN closure is overall attainable with an average overprediction bias of 36%, by simply assuming it to be composed of pure ammonium sulfate. Accounting for the internally mixed particle soluble volume fraction, estimated from the sulfate and organic mass loadings, reduces the average overprediction bias to 3%. Even when the first-order behavior of CCN is well constrained by simple volume fraction assumptions, the scatter between predicted and observed CCN concentrations remains large. Simultaneous measurements of size-resolved composition and mixing state as well as surfactant properties of the

aerosol are required to reduce the uncertainty in CCN closure for such a heterogeneous mix of pollution sources. Contrary to ground-based measurements in the Houston area, the activation kinetics of the CCN are on average similar to ammonium sulfate, and do not suggest delays resulting from the presence of organics.

[46] **Acknowledgments.** We acknowledge support from the National Oceanic and Atmospheric Administration (NOAA) under contracts NA05OAR4310101 and NA06OAR4310082, the support of an NSF CAREER grant, and the Office of Naval Research. S.L. would like to acknowledge the support of a Georgia Institute of Technology (Georgia Tech) Presidential Fellowship, a National Center for Atmospheric Research (NCAR) Advanced Study Program (ASP) Graduate Fellowship, and a National Research Council Research Associateships Program Fellowship (awarded January 2008). We also thank C. Brock and three anonymous reviewers for helpful comments, as well as A. Stohl and S. Ekhardt for providing the Flexpart back trajectory results. M.K.D. and C.M. thank LANL-LDRD and DOE-Office of Science-OBER-ASP for support of the photoacoustic deployment.

References

- Arnott, W. P., and H. Moosmüller (1998), Real time, in situ measurement of aerosol light absorption with a new photoacoustic instrument, *Instrum. Aerosp. Ind.*, **44**, 713.
- Arnott, W. P., et al. (1999), Photoacoustic spectrometer for measuring light absorption by aerosol: Instrument description, *Atmos. Environ.*, **33**(17), 2845, doi:10.1016/S1352-2310(98)00361-6.
- Arnott, W. P., J. W. Walker, H. Moosmüller, R. A. Elleman, H. H. Jonsson, G. Buzorius, W. C. Conant, R. C. Flagan, and J. H. Seinfeld (2006), Photoacoustic insight for aerosol light absorption aloft from meteorological aircraft and comparison with particle soot absorption photometer measurements: DOE Southern Great Plains climate research facility and the coastal stratocumulus imposed perturbation experiments, *J. Geophys. Res.*, **111**, D05S02, doi:10.1029/2005JD005964.
- Asa-Awuku, A., A. Nenes, A. P. Sullivan, C. J. Hennigan, and R. J. Weber (2008), Investigation of molar volume and surfactant characteristics of water-soluble organic compounds in biomass burning aerosol, *Atmos. Chem. Phys.*, **8**, 799–812.
- Asa-Awuku, A., G. J. Engelhart, B. H. Lee, S. N. Pandis, and A. Nenes (2009), Relating CCN activity, volatility, and droplet growth kinetics of β -caryophyllene secondary organic aerosol, *Atmos. Chem. Phys.*, **9**, 795–812.
- Broekhuizen, K., R. Y. W. Chang, W. R. Leitch, S. M. Li, and J. P. D. Abbatt (2006), Closure between measured and modeled cloud condensation nuclei (CCN) using size-resolved aerosol compositions in downtown Toronto, *Atmos. Chem. Phys.*, **6**, 2513–2524.
- Cantrell, W., G. Shaw, G. R. Cass, Z. Chowdhury, L. S. Hughes, K. A. Prather, S. A. Guazzotti, and K. R. Coffee (2001), Closure between aerosol particles and cloud condensation nuclei at Kaashidhoo Climate Observatory, *J. Geophys. Res.*, **106**(D22), 28,711–28,718, doi:10.1029/2000JD900781.
- Chan, M. N., S. M. Kreidenweis, and C. K. Chan (2008), Measurements of the hygroscopic and deliquescence properties of organic compounds of different solubilities in water and their relationship with cloud condensation nuclei activities, *Environ. Sci. Technol.*, **42**, 3602–3608, doi:10.1021/es7023252.
- Chang, R. Y.-W., P. S. K. Liu, W. R. Leitch, and J. P. D. Abbatt (2007), Comparison between measured and predicted CCN concentrations at Egbert, Ontario: Focus on the organic aerosol fraction at a semi-rural site, *Atmos. Environ.*, **41**(37), 8172–8182, doi:10.1016/j.atmosenv.2007.06.039.
- Cubison, M. J., B. Ervens, G. Feingold, K. S. Docherty, I. M. Ulbrich, L. Shields, K. Prather, S. Hering, and J. L. Jimenez (2008), The influence of chemical composition and mixing state of Los Angeles urban aerosol on CCN number and cloud properties, *Atmos. Chem. Phys.*, **8**, 5649–5667.
- Decesari, S., M. C. Facchini, S. Fuzzi, G. B. McFiggans, H. Coe, and K. N. Bower (2005), The water-soluble organic component of size-segregated aerosol, cloud water and wet depositions from Jeju Island during ACE-Asia, *Atmos. Environ.*, **39**, 211–222, doi:10.1016/j.atmosenv.2004.09.049.
- Dinar, E., T. F. Mentel, and Y. Rudich (2006), The density of humic acids and humic like substances (HULIS) from fresh and aged wood burning and pollution aerosol particles, *Atmos. Chem. Phys.*, **6**, 5213–5224.
- Dinar, E., T. Anttila, and Y. Rudich (2008), CCN activity and hygroscopic growth of organic aerosols following reactive uptake of ammonia, *Environ. Sci. Technol.*, **42**, 793–799, doi:10.1021/es071874p.
- Drewnick, F., et al. (2005), A new time-of-flight aerosol mass spectrometer (TOF-AMS)—Instrument description and first field deployment, *Aerosol Sci. Technol.*, **39**, 637–658, doi:10.1080/02786820500182040.
- Dusek, U., et al. (2006), Size matters more than chemistry for cloud-nucleating ability of aerosol particles, *Science*, **312**, 1375–1378.
- Engelhart, G. J., A. Asa-Awuku, A. Nenes, and S. N. Pandis (2008), CCN activity and droplet growth kinetics of fresh and aged monoterpene secondary organic aerosol, *Atmos. Chem. Phys.*, **8**, 3937–3949.
- Ervens, B., M. Cubison, E. Andrews, G. Feingold, J. A. Ogren, J. L. Jimenez, P. DeCarlo, and A. Nenes (2007), Prediction of cloud condensation nucleus number concentration using measurements of aerosol size distributions and composition and light scattering enhancement due to humidity, *J. Geophys. Res.*, **112**, D10S32, doi:10.1029/2006JD007426.
- Facchini, M. C., S. Decesari, M. Mircea, S. Fuzzi, and G. Logglio (2000), Surface tension of atmospheric wet aerosol and cloud/fog droplets in relation to their organic carbon content and chemical composition, *Atmos. Environ.*, **34**(28), 4853–4857, doi:10.1016/S1352-2310(00)00237-5.
- Forster, P., et al. (2007), Changes in atmospheric constituents and in radiative forcing, in *Climate Change 2007: The Physical Science Basis*, pp. 131–234, Cambridge Univ. Press, Cambridge, U. K.
- Furutani, H., M. Dall'osto, G. C. Roberts, and K. A. Prather (2008), Assessment of the relative importance of atmospheric aging on CCN activity derived from field observations, *Atmos. Environ.*, **42**(13), 3130–3142, doi:10.1016/j.atmosenv.2007.09.024.
- Hegg, D. A., D. S. Covert, P. A. Covert, and H. Jonsson (2005), Determination of the efficiency of an aircraft aerosol inlet, *Aerosol Sci. Technol.*, **39**, 966–971, doi:10.1080/02786820500377814.
- Hinds, W. C. (1999), *Properties, Behavior, and Measurement of Airborne Particles*, John Wiley, Hoboken, N. J.
- Lance, S., J. Medina, J. N. Smith, and A. Nenes (2006), Mapping the operation of the DMT continuous flow CCN counter, *Aerosol Sci. Technol.*, **40**, 242–254, doi:10.1080/02786820500543290.
- Lu, M.-L., G. Feingold, H. H. Jonsson, P. Y. Chuang, H. Gates, R. C. Flagan, and J. H. Seinfeld (2008), Aerosol-cloud relationships in continental shallow cumulus, *J. Geophys. Res.*, **113**, D15201, doi:10.1029/2007JD009354.
- Medina, J., A. Nenes, R. E. P. Sotiropoulou, L. D. Cottrell, L. D. Ziemba, P. J. Beckman, and R. J. Griffin (2007), Cloud condensation nuclei closure during the International Consortium for Atmospheric Research on Transport and Transformation 2004 campaign: Effects of size-resolved composition, *J. Geophys. Res.*, **112**, D10S31, doi:10.1029/2006JD007588.
- Mikhailov, E. F., S. S. Vlasenko, I. A. Podgorny, V. Ramanathan, and C. E. Corrigan (2006), Optical properties of soot-water drop agglomerates: An experimental study, *J. Geophys. Res.*, **111**, D07209, doi:10.1029/2005JD006389.
- Mircea, M., et al. (2005), Importance of the organic aerosol fraction for modeling aerosol hygroscopic growth and activation: A case study in the Amazon Basin, *Atmos. Chem. Phys.*, **5**, 3111–3126.
- Moosmüller, H., et al. (1998), Photoacoustic and filter measurements related to aerosol light absorption during the Northern Front Range Air Quality Study (Colorado 1996/1997), *J. Geophys. Res.*, **103**(D21), 28,149–28,157, doi:10.1029/98JD02618.
- Murphy, S. M., et al. (2009), Comprehensive simultaneous shipboard and airborne characterization of exhaust from a modern container ship at sea, *Environ. Sci. Technol.*, **43**, 4626–4640, doi:10.1021/es802413j.
- Noone, K. J., J. A. Ogren, J. Heintzenberg, R. J. Charlson, and D. S. Covert (1988), Design and calibration of a counterflow virtual impactor for sampling of atmospheric fog and cloud droplets, *Aerosol Sci. Technol.*, **8**, 235–244, doi:10.1080/02786828808959186.
- Ogren, J. A., J. Heintzenberg, A. Zuber, K. J. Noone, and R. J. Charlson (1992), Measurements of the size-dependence of non-volatile aqueous mass concentrations in cloud droplets, *Tellus, Ser. B*, **41**, 24–31.
- Padró, L. T., A. Asa-Awuku, R. Morrison, and A. Nenes (2007), Inferring thermodynamic properties from CCN activation experiments: Single-component and binary aerosols, *Atmos. Chem. Phys.*, **7**, 5263–5274.
- Petters, M. D., and S. M. Kreidenweis (2007), A single parameter representation of hygroscopic growth and CNN activity, *Atmos. Chem. Phys.*, **7**, 1961–1971.
- Quinn, P. K., T. S. Bates, D. J. Coffman, and D. S. Covert (2008), Influence of particle size and chemistry on the cloud nucleating properties of aerosols, *Atmos. Chem. Phys.*, **8**, 1029–1042.
- Roberts, G., and A. Nenes (2005), A continuous-flow longitudinal thermal-gradient CCN chamber for atmospheric measurements, *Aerosol Sci. Technol.*, **39**, 206–221, doi:10.1080/027868290913988.
- Rose, D., S. S. Gunthe, E. Mikhailov, G. P. Frank, U. Dusek, M. O. Andreae, and U. Poschl (2008), Calibration and measurement uncertainties of a continuous-flow cloud condensation nuclei counter (DMT-

- CCNC): CCN activation of ammonium sulfate and sodium chloride aerosol particles in theory and experiment, *Atmos. Chem. Phys.*, *8*, 1153–1179.
- Ruehl, C. R., P. Y. Chuang, and A. Nenes (2008), How quickly do cloud droplets form on atmospheric particles, *Atmos. Chem. Phys.*, *8*, 1043–1055.
- Salcedo, D. (2006), Equilibrium phase diagrams of aqueous mixtures of malonic acid and sulfate/ammonium salts, *J. Phys. Chem.*, *110*, 12,158–12,165.
- Saxena, P., and L. M. Hildemann (1996), Water-soluble organics in atmospheric particles: A critical review of the literature and application of thermodynamics to identify candidate compounds, *J. Atmos. Chem.*, *24*, 57–109, doi:10.1007/BF00053823.
- Schwarz, J. P., et al. (2008), Measurement of the mixing state, mass and optical size of individual black carbon particles in urban and biomass burning emissions, *Geophys. Res. Lett.*, *35*, L13810, doi:10.1029/2008GL033968.
- Seinfeld, J. H., and S. N. Pandis (2006), *Atmospheric Chemistry and Physics: From Air Pollution to Climate Change*, 2nd ed., John Wiley, Hoboken, N. J.
- Shulman, M. L., M. C. Jacobson, R. J. Carlson, R. E. Synoveca, and T. E. Young (1996), Dissolution behavior and surface tension effects of compounds in nucleating cloud droplets, *Geophys. Res. Lett.*, *23*(3), 277–280, doi:10.1029/95GL03810.
- Slowik, J. G., K. Stainken, P. Davidovits, L. R. Williams, J. T. Jayne, C. E. Kolb, D. R. Worsnop, Y. Rudich, P. F. DeCarlo, and J. L. Jimenez (2004), Particle morphology and density characterization by combined mobility and aerodynamic diameter measurements. Part 2: Application to combustion-generated soot aerosols as a function of fuel equivalence ratio, *Aerosol Sci. Technol.*, *38*, 1206–1222, doi:10.1080/027868290903916.
- Sorooshian, A., S. M. Murphy, S. Hersey, H. Gates, L. T. Padro, A. Nenes, F. J. Brechtel, H. Jonsson, R. C. Flagan, and J. H. Seinfeld (2008a), Comprehensive airborne characterization of aerosol from a major bovine source, *Atmos. Chem. Phys.*, *8*, 5489–5520.
- Sorooshian, A., S. Hersey, F. J. Brechtel, A. Corless, R. C. Flagan, and J. H. Seinfeld (2008b), Rapid, size-resolved aerosol hygroscopic growth measurements: Differential aerosol sizing and hygroscopicity spectrometer probe (DASH-SP), *Aerosol Sci. Technol.*, *42*, 445–464, doi:10.1080/02786820802178506.
- VanReken, T. M., T. A. Rissman, G. C. Roberts, V. Varutbangkul, H. H. Jonsson, R. C. Flagan, and J. H. Seinfeld (2003), Toward aerosol/cloud condensation nuclei (CCN) closure during CRYSTAL-FACE, *J. Geophys. Res.*, *108*(D20), 4633, doi:10.1029/2003JD003582.
- Vestin, A., et al. (2007), Cloud-nucleating properties of the Amazonian biomass burning aerosol: Cloud condensation nuclei measurements and modeling, *J. Geophys. Res.*, *112*, D14201, doi:10.1029/2006JD008104.
- Wang, J. (2007), Effects of spatial and temporal variations in aerosol properties on mean cloud albedo, *J. Geophys. Res.*, *112*, D16201, doi:10.1029/2007JD008565.
- Wang, J., R. C. Flagan, and J. H. Seinfeld (2003), A differential mobility analyzer DMA system for submicron aerosol measurements at ambient relative humidity, *Aerosol Sci. Technol.*, *37*, 46–52, doi:10.1080/02786820300891.
- Wang, J., Y.-N. Lee, P. H. Daum, J. Jayne, and M. L. Alexander (2008), Effects of aerosol organics on cloud condensation nucleus (CCN) concentration and first indirect aerosol effect, *Atmos. Chem. Phys.*, *8*, 6325–6339.
- Zelenyuk, A., Y. Cai, and D. Imre (2006), From agglomerates of spheres to irregularly shaped particles: Determination of dynamic shape factors from measurements of mobility and vacuum aerodynamic diameters, *Aerosol Sci. Technol.*, *40*, 197–217, doi:10.1080/02786820500529406.
-
- M. K. Dubey, Climate Observations, Los Alamos National Laboratory, MS-D462, Los Alamos, NM 87545, USA.
- G. Feingold, Chemical Sciences Division, National Oceanic and Atmospheric Administration, MS R/CSD2, 325 Broadway, Boulder, CO 80305, USA.
- R. C. Flagan, H. Gates, S. M. Murphy, T. A. Rissman, J. H. Seinfeld, A. Sorooshian, and V. Varutbangkul, Department of Chemical Engineering, California Institute of Technology, 1200 East California Boulevard, MC 210-41, Pasadena, CA 91125, USA.
- H. H. Jonsson, Center for Inter-Disciplinary Remotely Piloted Aircraft Studies, Naval Postgraduate School, 3200 Imjin Road, Marina, CA 93933, USA.
- S. Lance and A. Nenes, School of Earth and Atmospheric Sciences, Georgia Institute of Technology, 311 Ferst Drive, Atlanta, GA 30332, USA. (athanasios.nenes@gatech.edu)
- C. Mazzoleni, Department of Physics, Michigan Technological University, 1400 Townsend Drive, Houghton, MI 49931, USA.